NAVAL POSTGRADUATE SCHOOL
Monterey, California

THESIS

EXPERIMENTAL STUDIES OF WELDING EFFECTS ON DAMPING FOR UNDERSEA WARFARE APPLICATIONS

by

Agustin E. Carey

September 2002

Thesis Advisor: Young W. Kwon
Co-Advisor: Young S. Shin

Approved for public release; distribution is unlimited

THIS PAGE INTENTIONALLY LEFT BLANK

REPORT DOCUMENTATION PAGE			Form Approved OMB No. 0704-0188
Public reporting burden for this collection of information is estimated to average 1 hour per response, including the time for reviewing instruction, searching existing data sources, gathering and maintaining the data needed, and completing and reviewing the collection of information. Send comments regarding this burden estimate or any other aspect of this collection of information, including suggestions for reducing this burden, to Washington headquarters Services, Directorate for Information Operations and Reports, 1215 Jefferson Davis Highway, Suite 1204, Arlington, VA 22202-4302, and to the Office of Management and Budget, Paperwork Reduction Project (0704-0188) Washington DC 20503.			
1. AGENCY USE ONLY ***(Leave blank)***	**2. REPORT DATE** May 2000	**3. REPORT TYPE AND DATES COVERED** Master's Thesis	
4. TITLE AND SUBTITLE: Experimental Studies of Welding Effects on Damping for Undersea Warfare Applications			**5. FUNDING NUMBERS**
6. AUTHOR(S) Agustin E Carey			
7. PERFORMING ORGANIZATION NAME(S) AND ADDRESS(ES) Naval Postgraduate School Monterey, CA 93943-5000			**8. PERFORMING ORGANIZATION REPORT NUMBER**
9. SPONSORING /MONITORING AGENCY NAME(S) AND ADDRESS(ES) N/A			**10. SPONSORING/MONITORING AGENCY REPORT NUMBER**
11. SUPPLEMENTARY NOTES The views expressed in this thesis are those of the author and do not reflect the official policy or position of the Department of Defense or the U.S. Government.			
12a. DISTRIBUTION / AVAILABILITY STATEMENT Approved for public release; distribution is unlimited			**12b. DISTRIBUTION CODE**

13. ABSTRACT ***(maximum 200 words)***

Damping in structures has historically been of great importance in nearly all branches of engineering endeavors, and it also happens to be one of the most difficult parameters to predict. The purpose of this research is to study the effects that welding has on damping. Measurements and comparisons of the damping ratios of two welded stiffened plates, two flat plates and one machined stiffened plate are undertaken. The frequency response and natural frequencies of five steel structures are determined experimentally. A finite element model is created for three of the structures to determine the natural frequencies and associated mode shapes. The damping ratios are then determined using the half-power point method.

The results show that at frequencies less than 500 Hz, welding tends to cause the damping ratio to increase. The experimental and numerical results show that the mode shapes that experience the highest degree of stress at a weld are associated with the natural frequencies with the highest damping ratio. These results may lend to better understanding of the effects of welding on damping and assist in obtaining better empirical approximations of damping for use in ship shock computer simulations.

14. SUBJECT TERMS Vibration, Damping, Welding			**15. NUMBER OF PAGES** 72
			16. PRICE CODE
17. SECURITY CLASSIFICATION OF REPORT Unclassified	**18. SECURITY CLASSIFICATION OF THIS PAGE** Unclassified	**19. SECURITY CLASSIFICATION OF ABSTRACT** Unclassified	**20. LIMITATION OF ABSTRACT** UL

NSN 7540-01-280-5500 Standard Form 298 (Rev. 2-89)
Prescribed by ANSI Std. 239-18

THIS PAGE INTENTIONALLY LEFT BLANK

Approved for public release; distribution is unlimited

EXPERIMENTAL STUDIES OF WELDING EFFECTS ON DAMPING FOR UNDERSEA WARFARE APPLICATIONS

Agustin E. Carey
Lieutenant, United States Navy
B.S.C.E, University of Texas at Austin, 1995

Submitted in partial fulfillment of the
requirements for the degree of

MASTER OF SCIENCE IN MECHANICAL ENGINEERING

from the

NAVAL POSTGRADUATE SCHOOL
September 2002

Author: Agustin E. Carey

Approved by: Young W. Kwon
Thesis Advisor

Young S. Shin
Co-Advisor

Young W. Kwon
Chairman, Department of Mechanical Engineering

THIS PAGE INTENTIONALLY LEFT BLANK

ABSTRACT

Damping in structures has historically been of great importance in nearly all branches of engineering endeavors, and it also happens to be one of the most difficult parameters to predict. The purpose of this research is to study the effects that welding has on damping. Measurements and comparisons of the damping ratios of two welded stiffened plates, two flat plates and one machined stiffened plate are undertaken. The frequency response and natural frequencies of five steel structures are determined experimentally. A finite element model is created for three of the structures to determine the natural frequencies and associated mode shapes. The damping ratios are then determined using the half-power point method.

The results show that at frequencies less than 500 Hz, welding tends to cause the damping ratio to increase. The experimental and numerical results show that the mode shapes that experience the highest degree of stress at a weld are associated with the natural frequencies with the highest damping ratio. These results may lend to better understanding of the effects of welding on damping and assist in obtaining better empirical approximations of damping for use in ship shock computer simulations.

THIS PAGE INTENTIONALLY LEFT BLANK

TABLE OF CONTENTS

I. INTRODUCTION....1
A. BACKGROUND....1
B. OBJECTIVES....5
C. TEST SPECIMEN DESCRIPTION....5

II. THEORY....9
A. FORCED VIBRATION....9
B. HALF-POWER POINT METHOD....11

III. EXPERIMENTAL SETUP....15
A. EQUIPMENT SETUP....15
1. Impact Testing....15
2. Shaker Testing....17
3. Exciter Testing....19
B. NUMERICAL SIMULATIONS....22

IV. RESULTS AND DISCUSSION....25
A. IMPACT TESTING....25
B. SHAKER TESTING....26
1. Flat Plate....26
2. Welded Stiffened Plate....28
3. Machined Stiffened Plate....29
C. EXCITER TESTING....30
1. Flat Plate....31
2. Stiffened Plate....35
D. NUMERICAL RESULTS....38

V. TEST COMPARISONS....43

IV. CONCLUSIONS AND RECOMMENDATIONS....49

LIST OF REFERENCES....51

INITIAL DISTRIBUTION LIST....53

THIS PAGE INTENTIONALLY LEFT BLANK

LIST OF FIGURES

Figure 1. Process of damping identification and analytical model correction (From: Ref. 4) 3
Figure 2. Unit Damping Energy vs. Stress Amplitude (From: Ref. 7)....4
Figure 3. 18-inch test specimens (a) flat plate (b) upper right welded plate, lower right machined plate 6
Figure 4. 8.5-foot test structures (a) flat plate (b) stiffened plate....7
Figure 5. Half-power points (After: Ref.9) 13
Figure 6. Machined stiffened plate supported during impact testing....15
Figure 7. Equipment setup using the Piezotronics Modally Tuned Impact Hammer. 16
Figure 8. Location of drilled hole and measurement points used for test structures....17
Figure 9. Flat plate test structure set up on Wilcoxon Generator....18
Figure 10. Equipment setup using the Wilcoxon Research Model F4 Electromagnetic Shaker. Input signal: force gage Output signal: accelerometer 18
Figure 11. Equipment setup using the Wilcoxon Research Model F4 Electromagnetic Shaker. Input signal: accelerometer Output signal: external transducer....19
Figure 12. Schematic of sensor locations. Force sensor location: I1 Accelerometer locations A, B, C, D, I2....20
Figure 13. MB Dynamics Modal 50 Exciter Setup....20
Figure 14. Modal 50 Exciter and Test Structure Setup....21
Figure 15. Test structure setup using cardboard box and sand 22
Figure 16. Schematic of sensor locations. Force sensor location: I1 Accelerometer locations A, B, C, D, E, F, I2....22
Figure 17. Typical coherence response obtained during testing of flat plate, welded stiffened plate, and machined stiffened plate....26
Figure 18. Sample frequency response of flat plate, input and output measured at the generator 27
Figure 19. Sample resonance peak used to determine damping ratio 27
Figure 20. Sample frequency response of welded stiffened plate. Accelerometer on generator used as input, external accelerometer positioned at location A used as output....29
Figure 21. Sample frequency response of machined stiffened plate. Accelerometer on generator used as input, external accelerometer positioned at location A used as output....30
Figure 22. Frequency response of 8.5-foot flat plate using MB Dynamics exciter with force sensor uses as the input and output at location C 31
Figure 23. Frequency response of flat plate using MB Dynamics exciter with accelerometer at location I1 as the input and output at location C 32
Figure 24. Frequency response of 8.5-foot plate inserted in sand with force sensor at location I1 as the input and output at location C 34
Figure 25. Frequency response of 8.5-foot stiffened plate with force sensor at location I1 as the input and accelerometer at location C as the output. 35

Figure 26. Frequency response of 8.5-foot stiffened plate with accelerometer at location I1 as the input and accelerometer at location C as the output.....36
Figure 27. Frequency response of 8.5-foot stiffened plate inserted in sand with force sensor at location I1 as the input and output at location C 37
Figure 28. Mode shapes for 18-inch flat plate (a) 4^{th} mode shape (b) 5^{th} mode shape 39
Figure 29. Mode shapes for 18-inch stiffened plate (a) 2^{nd} mode shape (b) 4^{th} mode shape40
Figure 30. Mode shapes of 8.5-foot stiffened plate (a) 6^{th} mode shape (b) 10^{th} mode shape (c) 12^{th} mode shape 41
Figure 31. Damping Ratio vs. Frequency response for the flat plate, welded stiffened plated, and machined stiffened plate measured at the shaker. 43
Figure 32. Damping Ratio vs. Frequency response for the flat plate, welded stiffened plated, and machined stiffened plate measured at the location A.....44
Figure 33. Damping Ratio vs. Frequency response for the flat plate, welded stiffened plated, and machined stiffened plate measured at the location B. 44
Figure 34. Damping Ratio vs. Frequency response for 8.5-foot plates using the force sensor as the input signal and the accelerometer as the output signal. (a) measured at location A (b) measured at location B (c) measured at location C46
Figure 35. Damping Ratio vs. Frequency response for 8.5-foot plates using the accelerometers as the input and output signals. (a) measured at location A (b) measured at location B (c) measured at location C.....47
Figure 36. Damping Ratio vs. Frequency response for 8.5-foot plates with one end inserted in sand using the force sensor as the input and accelerometer as the output. (a) measured at location A (b) measured at location B (c) measured at location C (d) measured at location D (e) measured at location D (f) measured at location F.....48

LIST OF TABLES

Table 1. Properties and dimensions of 18-inch test specimens.....6
Table 2. Dimensions of 8.5-foot test structures 7
Table 3. Number of Shell Elements Used for Each Structure 23
Table 4. Natural frequencies and associated damping ratios for flat plate. Force gage and accelerometer on generator used as input and output, respectively 28
Table 5. Natural frequencies and associated damping ratios for flat plate. Force gage on generator used as input, external accelerometer used as output 28
Table 6. Natural frequencies and associated damping ratios for welded stiffened plate for the three different measurement locations. 29
Table 7. Natural frequencies and associated damping ratios for welded stiffened plate for the three different measurement locations 30
Table 8. Natural frequencies and damping ratios determined for the 8.5-foot flat plate using MB Dynamics exciter, force sensor at location I1 used as input 32
Table 9. Natural frequencies and damping ratios determined for 8.5-foot flat plate using the MB Dynamics exciter, accelerometer readings located at I2 used as input 33
Table 10. Natural frequencies and damping ratios determined for 8.5-foot flat plate with one end inserted into sand.....34
Table 11. Natural frequencies and damping ratios determined for 8.5-foot stiffened plate. Force sensor readings used as the input and the accelerometer readings used as the output.....36
Table 12. Natural frequencies and damping ratios determined for 8.5-foot stiffened plate. Accelerometer readings used as input and output signals.....37
Table 13. Natural frequencies and damping ratios determined for 8.5-foot stiffened plate with one end inserted into sand.....38
Table 14. Natural frequencies and mode shapes for each test structures.....38

THIS PAGE INTENTIONALLY LEFT BLANK

LIST OF SYMBOLS

$\bar{\lambda}$	Eigenvalue of improved model
p_k	Vector of unknown design variable changes
ϕ_a	Eigenvector of analytical model
ϕ_x	Eigenvector of experimental model
λ_x	Eigenvalue of experimental model
$[H]$	Damping matrix
m	Mass of the system
c	Damping of the system
k	Stiffness of the system
x	Displacement of the system
$\dot{x}$	Velocity of the system
$\ddot{x}$	Acceleration of the system
$H(\omega)$	Frequency response function
$F(t)$	Force applied to the system
ω_n	Natural frequency
ζ	Damping ratio
c_c	Critical damping coefficient
$[M]$	Mass matrix
$[C]$	Damping matrix
$[K]$	Stiffness matrix
ω_1, ω_2	Half-power points

THIS PAGE INTENTIONALLY LEFT BLANK

ACKNOWLEDGMENTS

I would like to extend sincere thanks and gratitude to Professors Young W. Kwon and Young S. Shin for their guidance and support throughout the preparation and completion of this thesis. Their patience and mentoring made this work both challenging and rewarding.

Additionally, I would like to thank my wife Epiphany and daughter Xenia for their patience and support during the countless hours spent earning my Masters Degree. Without their unconditional love and unwavering support this thesis would not have been possible.

THIS PAGE INTENTIONALLY LEFT BLANK

I. INTRODUCTION

A. BACKGROUND

Damping in structures has historically been of great importance in nearly all branches of engineering endeavors. Of particular interest to the Navy is damping in a ship structure. Unfortunately, damping can be one of the most difficult issues to deal with in structural dynamics perhaps because it is not as intuitive a concept as stiffness or mass. Perhaps this is why very little work has been done to predict the structural damping in structures. An understanding of the mechanisms that cause damping is crucial to predicting damping in structures.

Grice and Pinnington [1] developed a method for the vibration analysis of built-up structures. A ship is thought of as a collection of large beams and flexible plates, the beams making up the frame and the flexible plates making up the hull and deck plates. A vibration source will create long-wavelength waves that control the power into and out of the structure. Since the wave speed in the beams is high, it is reasonable to expect them to form the primary path for vibration transmission. As these long-waves travel along the beam, they form short-wavelength waves in the attached flexible plates. The long-waves thus transmit some of their energy to the short waves, making the flexural plates act like dampers. This is one mechanism for the development of damping. The method essentially models the stiff parts and flexible parts of a structure separately and then combines them to obtain the response of the complete structure. Grice [2] showed that the transmission of long flexural waves along the beam was strongly attenuated in narrow-frequency bands by the short flexural waves in the plate. Outside these narrow bands, transmission of the long wave was virtually unaffected by the plate. Prediction of these narrow bands would therefore provide a means for vibration control, hence damping. The theoretical foundation of the method was proven sound by testing a simple plate-stiffened beam attached to a large flexible plate [1]. Since the theoretical method can only be used for simple structures, Grice and Pinnington developed the method further by using a combination of numerical analysis to model the stiff part and analytical

impedances to model the flexible plate [3]. In both studies, predictions of input and transfer responses compared well with measurements.

Lin and his collogues [4], provide a method to identify a structural damping model by correlating the analytical mass and stiffness matrices developed by finite element methods with measured complex eigenvalues and eigenvectors of a test structure. The following equations represent the improved complex eigenvalue (1.1) and eigenvector (1.2) sensitivities:

$$\frac{\partial \bar{\lambda}_r}{\partial p_k} = \{\phi_a\}_r^T \frac{\partial [K]}{\partial p_k} \{\phi_x\}_r - (\lambda_x)_r \{\phi_a\}_r^T \frac{\partial [M]}{\partial p_k} \{\phi_x\}_r + j \{\phi_a\}_r^T \frac{\partial [H]}{\partial p_k} \{\phi_x\}_r \tag{1.1}$$

$$\frac{\partial \{\bar{\phi}\}_r}{\partial p_k} \equiv \{S_x\}_r = \sum_{i=1;i\neq r}^{N} \frac{\{\phi_a\}_i \{\phi_a\}_i^T}{(\lambda_x)_r (\lambda_x)_i} \times \left[\frac{\partial [K]}{\partial p_k} + j \frac{\partial [H]}{\partial p_k} - (\lambda_x)_r \frac{\partial [M]}{\partial p_k} \right] \{\phi_x\}_r - \frac{1}{2} \{\phi_a\}_r^T \frac{\partial [M]}{\partial p_k} \tag{1.2}$$

Equations (1.1) and (1.2) contain both the analytical and measured model data and are a better approximation of the complex slope of the eigenvalues between the analytical and experimental models, which is needed to identify the damping matrix and to correct the analytical mass and stiffness matrices [4]. The flow chart in Figure 1 illustrates the process of damping identification using the improved equations (1.1 and 1.2)

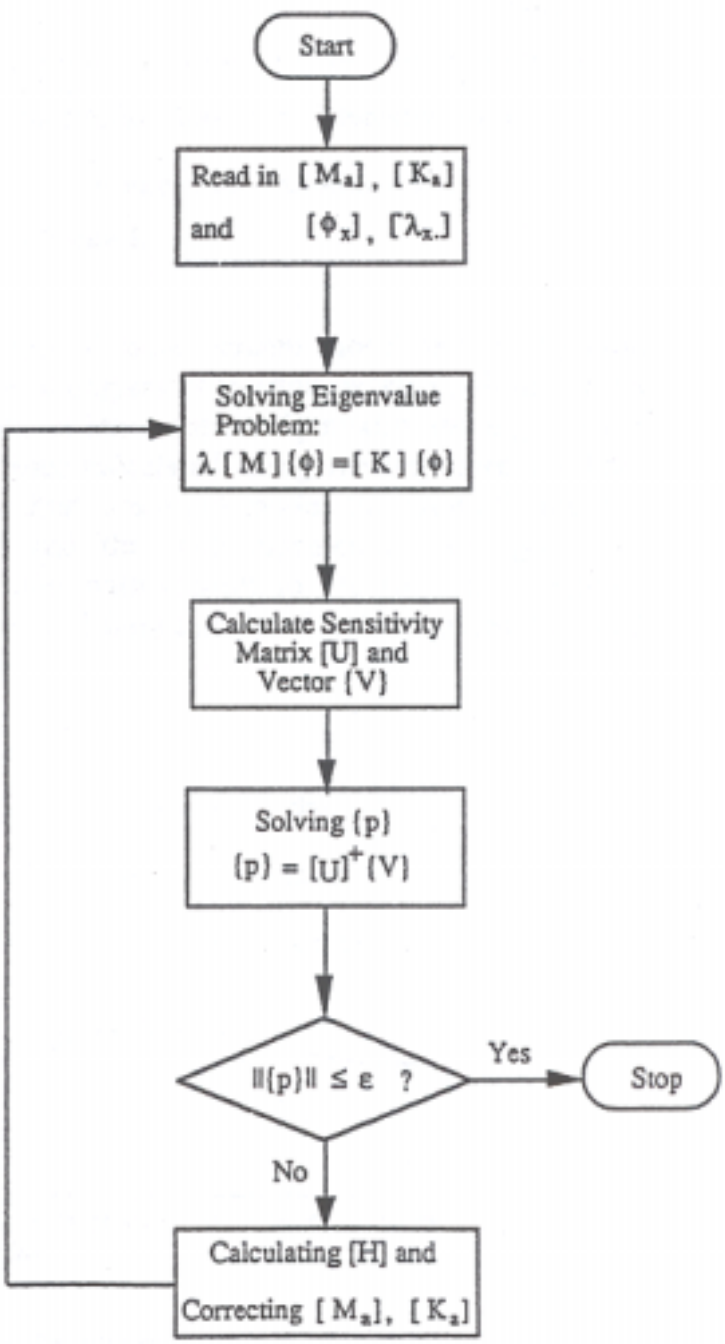

Figure 1. Process of damping identification and analytical model correction (From: Ref. 4)

Lin et al [Ref. 4] tested the applicability of the new equations by applying them to a frame structure modeled by 31 beam elements. To illustrate the accuracy of the equations, eigenvalue and eigenvector sensitivities were compared for the classical, improved and the exact results showing that the new equations are very accurate.

A comprehensive literature review revealed that two mechanisms that contribute largely to damping are friction at structural joints and welding effects together with stress concentrations. It has been found that 90% of the total damping of vibrational energy takes place in the structural joints [5,6,7]. Welded joints also exhibit considerable damping, less than the bolted joints but substantially more than solid materials, due in large part to slippage in members in contact not restrained fully by the weld [8]. But it is not clear how much welding effects contribute to damping.

Betts and his collogues conducted a survey of internal hull damping, and they concluded that welding effects together with stress concentrations were among the most important sources of hull damping in deformation modes [7]. Figure 2 shows a typical plot for the damping properties of mild steel in terms of the specific damping strain energy, for a wide range of stress amplitudes.

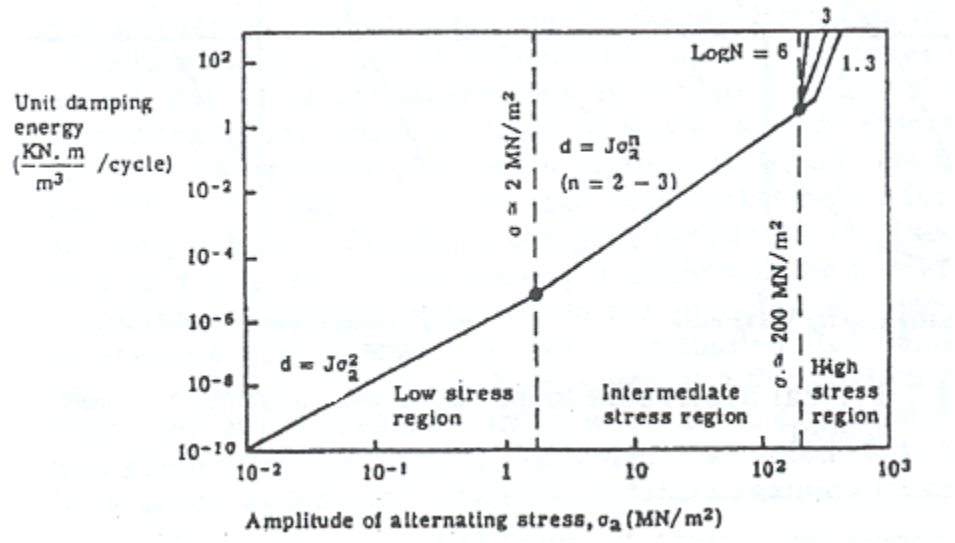

Figure 2. Unit Damping Energy vs. Stress Amplitude (From: Ref. 7)

Damping curves for other metallic materials generally have similar forms to those of mild steel. From the curve in Figure 2, as the stress amplitude increases, the damping energy increases. The primary effect of welding is from contraction of the weld upon cooling. This contraction causes tensile yield stresses in the material parallel and adjacent to the weld. The area of residual tensile yield stress at fillet welds usually extends for

approximately 3 to 4½ thickness either side of the weld, leaving some 10-15% of the plate material at tensile yield stress [7]. Welding and stress concentrations are often closely related in practice, such that high mean stress and alternating stress are often superimposed. Betts [Ref. 7] suggests that the residual stresses will frequently be in the plastic region which reinforces his view that welding effects together with stress concentrations are among the most important sources of hull damping. Since all modern day combatants are structurally welded together; an understanding of the welding effects is imperative to predicting structural damping.

B. OBJECTIVES

The objective of this research is to investigate the welding effects on damping in several beam-stiffened plates. The idea is to gain insight on how welding affects the damping of a ship structure, allowing for structural damping to be better defined in computer simulation. Having a better understanding of structural damping may assist the Navy in running better computer simulations of ship-shock trails which may one day lead to the abandonment of ship-shock trials altogether.

C. TEST SPECIMEN DESCRIPTION

The specimens were chosen in an attempt to simulate the structure of a ship, which can be thought of as a collection of beam stiffened plates. Therefore, for comparison three structures were chosen, a flat plate, a welded stiffened plate, and a machined stiffened plate. All specimens were made of A-36 steel. Table 1 lists the properties and dimensions of the specimens. A schematic of the test specimens is shown in Figure 3 along with a photo of each test specimen.

Table 1. Properties and dimensions of 18-inch test specimens

Modulus of Elasticity	29,000 ksi
Density	0.284 lb/in^3
Length	18 in
Width	8 in
T-beam height	1.6 in
T-beam width	1 in
Thickness	0.125 in

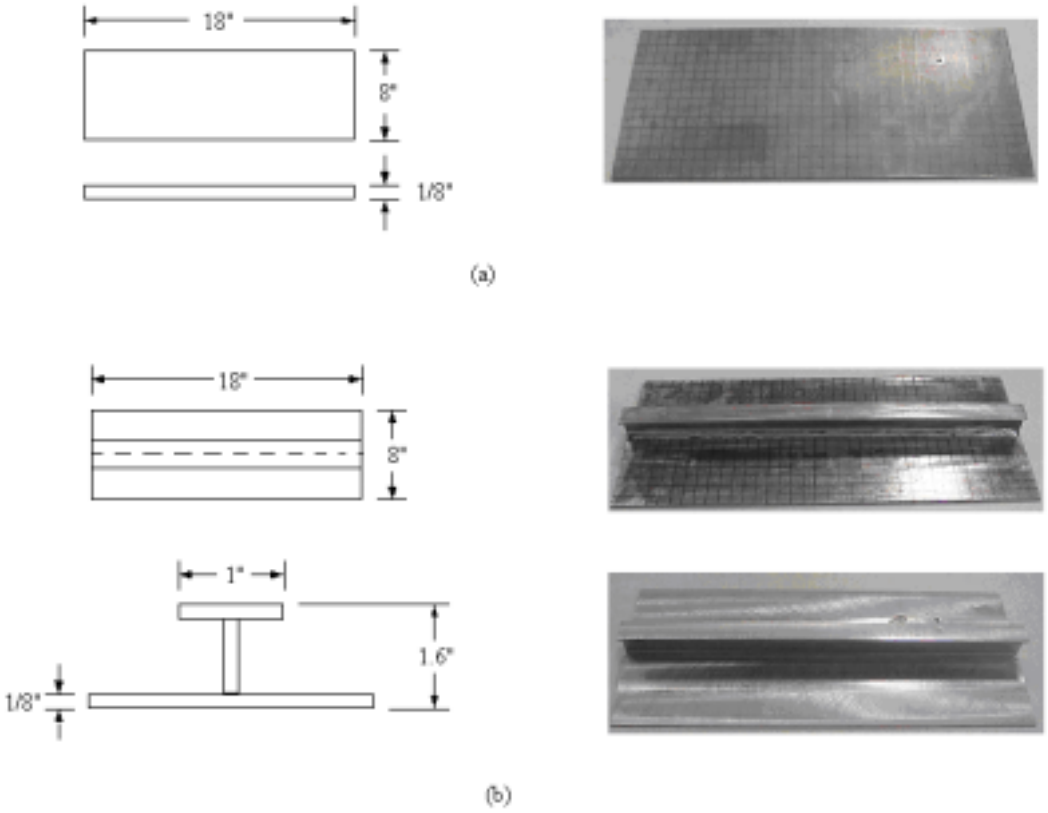

Figure 3. 18-inch test specimens (a) flat plate (b) upper right welded plate, lower right machined plate

After running tests and obtaining data on the three structures above, it was determined that larger test specimens were needed. The first structure was a simple flat plate, the second structure was a flat plat stiffened with four beams. A-36 steel was also used. Table 2 below lists the dimensions of the larger structures. Figure 4 shows a schematic of the 8.5-foot test structures along with a photo of each.

Table 2. Dimensions of 8.5-foot test structures

Plate Length	8.5 ft
Plate Width	18 in
Beam height	3.5 in
Beam Length	18 in
Plate Thickness	0.25 in
Beam Thickness	0.5 in

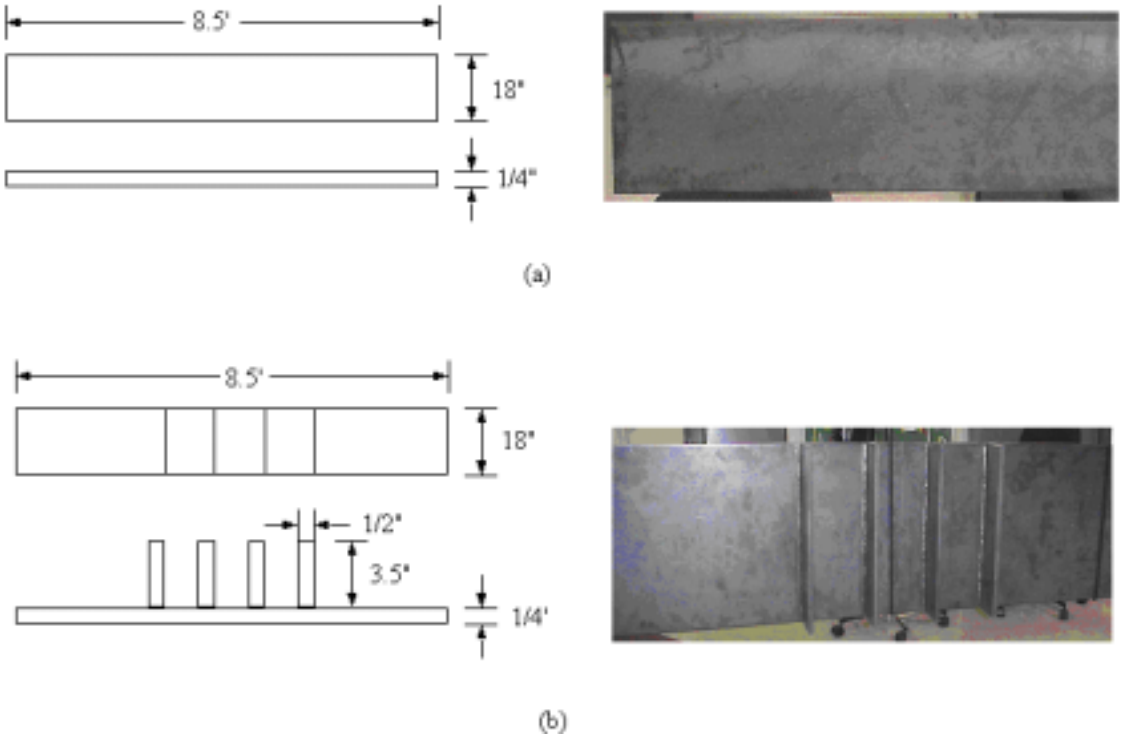

Figure 4. 8.5-foot test structures (a) flat plate (b) stiffened plate

THIS PAGE INTENTIONALLY LEFT BLANK

II. THEORY

A. FORCED VIBRATION

To accurately calculate the damping in a structure, its frequency response must first be determined in order to obtain the natural frequencies of the structure. In any linear system, there is a direct linear relationship between the input signal and the output signal; the ratio of this relationship is termed the frequency response function $H(\omega)$ [9].

For a single degree-of-freedom system (1-DOF), the equation of motion is given as:

$$m\ddot{x} + c\dot{x} + kx = F(t) \tag{2.1}$$

To solve the differential equation, we let the input $F(t) = e^{i\omega t}$, then the steady-state output becomes $x = H(\omega)e^{i\omega t}$, where ω is the frequency of the applied force and t is the time. By differentiating the steady-state output equation, expressions for the velocity and acceleration can be obtained. Substituting the displacement, velocity and acceleration expressions into equation (2.1) and canceling like terms, we obtain

$$(-m\omega^2 + ic\omega + k)H(\omega) = 1 \tag{2.2}$$

Then the frequency response equation becomes

$$H(\omega) = \frac{1}{k - m\omega^2 + ic\omega} \tag{2.3}$$

By factoring the stiffness from the denominator and substituting the following equations into equation (2.3),

$$\omega_n^2 = \frac{k}{m} \qquad \zeta = \frac{c}{c_c} = \frac{c}{2\sqrt{km}} \tag{2.4}$$

ω_n = Natural frequency

ζ = Damping ratio

c_c = Critical damping coefficient

the frequency response can then be written in its classical form:

$$H(\omega) = \frac{1}{1 - \left(\omega / \omega_n\right)^2 + i2\zeta\left(\omega / \omega_n\right)} \tag{2.5}$$

For a 1-DOF system, there is one natural frequency and one damping ratio associated with it. For multiple degrees-of-freedom (N-DOF), there are as many natural frequencies and damping ratios as there are DOF, so a system with 6-DOF will have six natural frequencies and six damping ratios. Modal analysis can be used to analyze a N-DOF system. The equation of motion for a N-DOF system in matrix form is:

$$[M]\{\ddot{x}\} + [C]\{\dot{x}\} + [K]\{x\} = \{F\} \tag{2.6}$$

The mass, damping, and stiffness matrices are n x n matrices, where n is the number of DOF in the system. The force, displacement, velocity and acceleration vectors are n by 1 in size. Each element in the vectors corresponds to a DOF of the system. The mass and stiffness matrixes are symmetric and may have some form of coupling. The first step to analyze the multi-DOF system is to determine the natural frequencies and mode shapes by analyzing the free response of the system. The general form of the free response of motion for a N-DOF system is as follows:

$$[M]\{\ddot{x}\} + [K]\{x\} = 0 \tag{2.7}$$

For each of the DOF we use $x = Xe^{i\omega t}$ and equation (2.7) reduces to:

$$\left[k_{ij} - m_{ij}\omega^2\right]\{x\} = 0 \qquad \text{where } i, j = 1...n \tag{2.8}$$

The indices i and j correspond to the element locations in the mass and stiffness matrices. From equation (2.8), a solution for the displacements is $\{x\} = 0$ if the matrix $\left[k_{ij} - m_{ij}\omega^2\right]$ is invertible. This solution, however, is the trivial solution. To ensure that the matrix is not invertible, the determinant of the matrix is forced to equal zero. By forcing the matrix determinant to equal zero, the matrix will now be singular and an inverse matrix does not exist, and therefore a non-trivial solution can be found. The above technique solves for the eigenvalues and eigenvectors of the matrix, which are the natural frequencies and mode shapes of the system, respectively. The mode shapes of a system illustrate how the system responds to an excitation at the corresponding natural

frequency. The first mode shape is associated with the lowest natural frequency; the second mode shape corresponds to the next lowest frequency and so forth. Placing the mode shape vectors as the columns of the matrix forms the modal matrix below:

$$[\Phi] = \left[\{\phi\}^1 \{\phi\}^2 ... \{\phi\}^n \right] \tag{2.9}$$

Φ is the modal matrix and ϕ are the mode shape vectors. The modal matrix will have the same number of rows and columns, as there are DOF's.

To decouple equation (2.6), we assume a set of modal coordinates;

$$\{x\} = [\Phi]\{q\}, \quad \{\dot{x}\} = [\Phi]\{\dot{q}\}, \quad \{\ddot{x}\} = [\Phi]\{\ddot{q}\} \tag{2.10}$$

We then substitute the above equations into equation (2.6) and multiply both sides by the transpose of the modal matrix.

$$[\Phi]^T [M][\Phi]\{\ddot{q}\} + [\Phi]^T [C][\Phi]\{\dot{q}\} + [\Phi]^T [K][\Phi]\{q\} = [\Phi]^T \{F\} \tag{2.11}$$

Using the orthogonal properties of the modal matrix and the symmetric properties of the mass, damping and stiffness matrix results in the following equation.

$$[\tilde{m}_{ii}]\{\ddot{q}\} + [\tilde{c}_{ii}]\{\dot{q}\} + [\tilde{k}_{ii}]\{q\} = [\Phi]^T \{F\} \tag{2.12}$$

The new modal mass, damping, and stiffness matrixes are diagonal. As a result, the modal coordinates are decoupled and can be solved for each DOF in the same manner as a 1-DOF system. Equation (2.12) can be further simplified by multiplying both sides by the inverse of the modal mass matrix [9], to get:

$$\begin{aligned} &\{\ddot{q}\} + [2\zeta_{ii}\omega_{ii}]\{\dot{q}\} + [\omega_{ii}^2]\{q\} = \{\tilde{F}\} \\ &\text{where } \{\tilde{F}\} = [\tilde{m}]^{-1} [\Phi]^T \{F\} \end{aligned} \tag{2.13}$$

B. HALF-POWER POINT METHOD

The damping ratio in equations (2.5 and 2.13) is calculated experimentally by using the half-power point method. The half-power point method determines the damping

ratio by examining the sharpness of the resonance peak. The following equation is the magnitude of the frequency response

$$H = \frac{1}{\sqrt{\left[1-\left(\omega/\omega_n\right)^2\right]^2 + \left[2\zeta\left(\omega/\omega_n\right)\right]^2}} \tag{2.14}$$

At resonance, the magnitude of the frequency response is $H_{res} = 1/2\zeta$. Taking the square of both sides of equation (2.14) to obtain:

$$\left(\frac{1}{2\zeta}\right)^2 = \frac{1}{\left[1-\left(\frac{\omega}{\omega_n}\right)^2\right]^2 + \left[2\zeta\left(\frac{\omega}{\omega_n}\right)\right]^2}$$

or (2.15)

$$\left(\frac{\omega}{\omega_n}\right)^4 - 2\left(1-2\zeta^2\right)\left(\frac{\omega}{\omega_n}\right)^2 + \left(1-8\zeta^2\right) = 0$$

Solving for $\left(\omega/\omega_n\right)^2$ results in the following equation.

$$\left(\omega/\omega_n\right)^2 = \left(1-2\zeta^2\right) \pm 2\zeta\sqrt{1-\zeta^2} \tag{2.16}$$

Assuming that ζ << 1, the higher order terms can be neglected, resulting in the following equation:

$$\left(\omega/\omega_n\right)^2 = 1 \pm 2\zeta \tag{2.17}$$

Letting ω_1 and ω_2 correspond to each of the frequencies in equation (2.17) and $\omega_2 > \omega_1$, equation (2.17) becomes:

$$4\zeta = \frac{\omega_2^2 - \omega_1^2}{\omega_n^2} \cong 2\left(\frac{\omega_2 - \omega_1}{\omega_n}\right) \tag{2.18}$$

The damping ratio can now be determined by rearranging equation (2.18)

$$\zeta = \frac{\omega_2 - \omega_1}{2\omega_n} = \frac{f_2 - f_1}{2 f_n} \tag{2.19}$$

Figure 5 illustrates how the half-power point method is utilized.

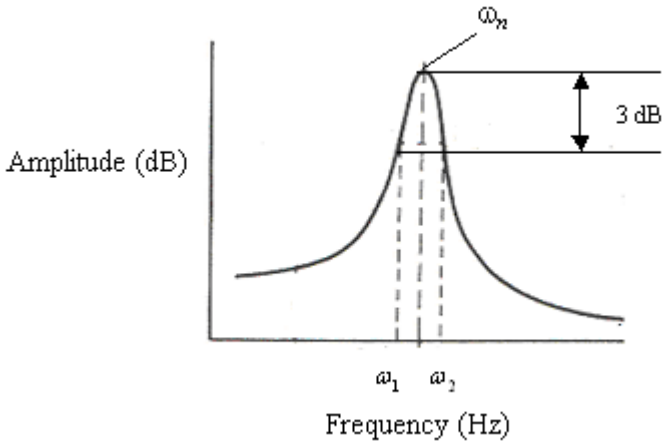

Figure 5. Half-power points (After: Ref.9)

THIS PAGE INTENTIONALLY LEFT BLANK

III. EXPERIMENTAL SETUP

Experimental testing was accomplished using three different setups. The smaller test structures (flat plate, welded stiffened plate, and machined stiffened plate) were analyzed using impact testing and shaker testing. The two large structures were analyzed using exciter testing.

A. EQUIPMENT SETUP

1. Impact Testing

For the impact testing, a PCB modally tuned impact hammer was used to excite the test structure while a PCB accelerometer (model 303A03) measured the structures response. The impact hammer test was used to determine the frequency response for the flat plate, welded stiffened plate, and machined stiffened plate. The first step in using the impact hammer was to choose the appropriate tip head. The rule of thumb is to choose a tip so that the amplitude of the force spectrum is no more than 3dB down at the maximum frequency of interest. The hard plastic tip was the only one that met this criterion for a frequency range of 2Hz to 1100Hz. To simulate a free hanging structure, the test structures were supported using bungee chords. Figure 6 shows the machined stiffened plate supported by the bungee chords. The test structures were impacted on the lower left corner, and accelerometer readings were taken at several locations on the test structure.

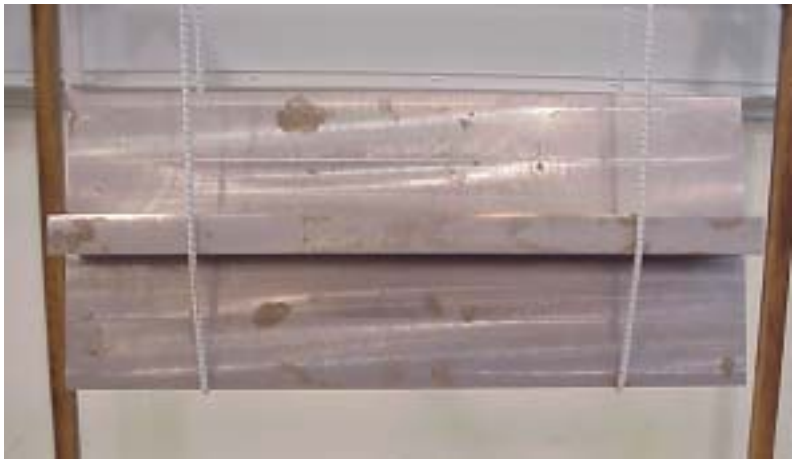

Figure 6. Machined stiffened plate supported during impact testing

The input signal was obtained from a force transducer located in the head of the impact hammer. The signal was amplified using a PCB Power unit (model 483B07) with the gain set at 1. The PCB power unit was also used to amplify the response signal, but the gain was set to a level of 10. The two signals were then analyzed using the Hewlett Packard 3562A Dynamic Signal Analyzer, where the frequency response, power spectra and coherency were measured. The HP 3562A Dynamic Signal Analyzer is a dual-channel, fast Fourier transform-based network, spectrum and waveform analyzer that provides analysis capabilities in both the time and frequency domains. The signal analyzer has a frequency resolution of 25.6 μHz allowing the user to obtain highly accurate, high-resolution plots of the frequency responses of the mechanical system. Single channel accuracy is ± 0.15 dB with 80 dB of dynamic range [10]. For transient or waveform analysis, signals can be sampled, digitized then stored in an internal memory, or directed via HP-IB to an external computer [10]. The stored waveforms can be recalled and analyzed in the time and frequency domains using MATLAB. The force-exponential window was used during the impact hammer test and 20 stable mean averages were used to obtain the correct frequency response. The time record was set to trigger when the input signal from the hammer reached 0.5 volts. Figure 7 shows the equipment setup for the impact testing.

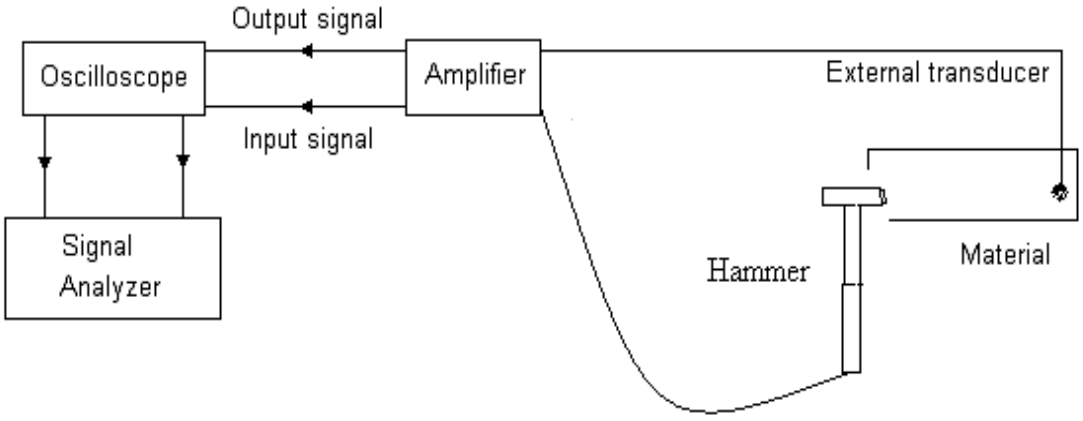

Figure 7. Equipment setup using the Piezotronics Modally Tuned Impact Hammer.

2. Shaker Testing

For the shaker testing, a Wilcoxon Research Model F7/F4 vibration generator was utilized to excite the structure. The vibration generator combines the use of an electromagnetic and a piezoelectric vibrating unit, which provide a controllable force output in the range of 10Hz to 15,000Hz [11]. The HP 3562A Dynamic Signal Analyzer was used to provide a 1V random noise input signal. The input signal was amplified using a Wilcoxon Research Power Amplifier (model PA7C). The input and output signals were determined by two methods. The first method was to use the force gage located in the generator as the input and the accelerometer located in the generator as the output. The second method was to use the accelerometer in the generator as the input and a PCB accelerometer (model 303A03), located at two random points as the output. Location of drilled hole and measurement points are shown in Figure 8.

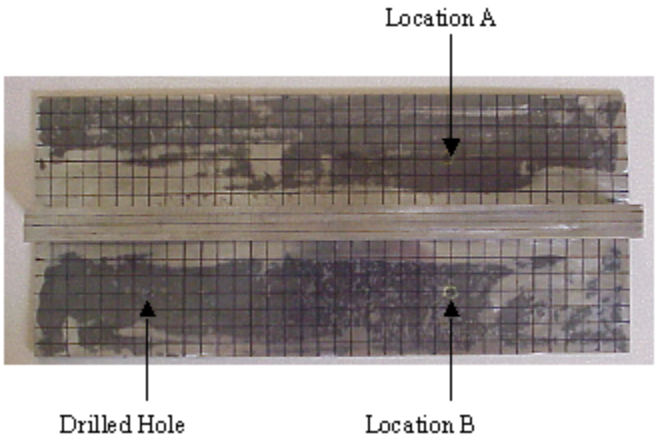

Figure 8. Location of drilled hole and measurement points used for test structures

A small hole was drilled off-center in the 18 inch flat plat, welded stiffened plate, and the machine stiffened plate. Each structure was then attached to the generator using a threaded stud and nut, while the ends were supported by bungee cords to simulate a free hanging structure. Figure 9 shows the above setup for the flat plate.

Figure 9. Flat plate test structure set up on Wilcoxon Generator

The input and output signals were then amplified using PCB Power unit (model 483B07) and fed to the HP 3562A Dynamic Signal Analyzer where the frequency response, power spectra and coherency were measured. The signal analyzer was set to the linear resolution mode using a Hann window. A stable mean of the frequency response was determined using 35 averages. The tests were conducted for a frequency span of 2 to 1100 Hz. Figures 10 and 11 are schematics of the equipment setup used to determine the frequency response of the material using the Wilcoxon Research F4/F7 vibration generator.

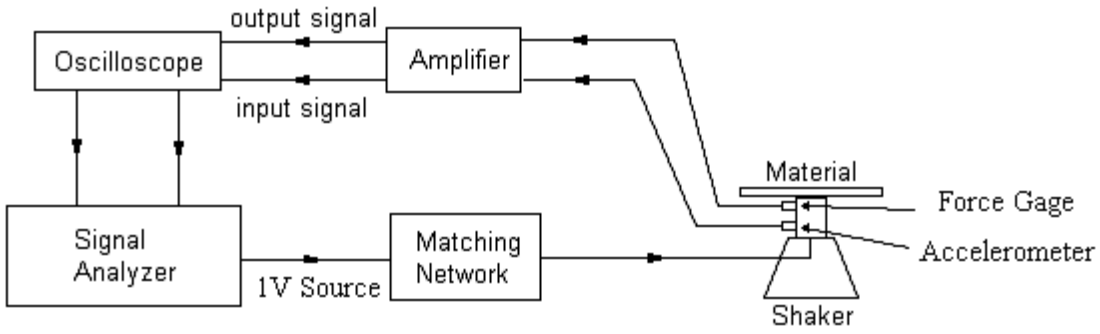

Figure 10. Equipment setup using the Wilcoxon Research Model F4 Electromagnetic Shaker. Input signal: force gage Output signal: accelerometer

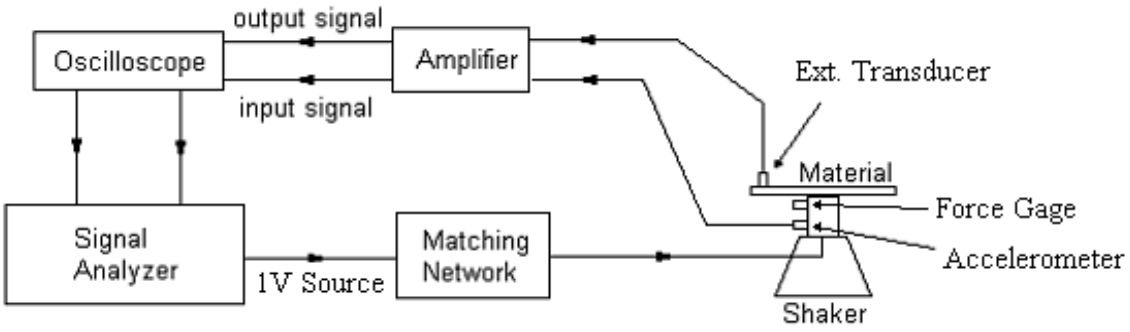

Figure 11. Equipment setup using the Wilcoxon Research Model F4 Electromagnetic Shaker. Input signal: accelerometer Output signal: external transducer

3. Exciter Testing

For the exciter testing, a MB Dynamics Modal 50 Exciter was used to excite the two 8.5-foot test structures. The HP 3562A Dynamic Signal Analyzer was used to provide a 500 mV random noise input signal. The input signal was amplified using a MB Dynamics Amplifier (model A SS250VCF). The exciter force was transmitted to the structure via a 10-32 stainless steel threaded rod attached to a PCB force sensor (model 208C01) and bolted to the structure. The force sensor has a measurement range of 10lb in tension and compression, a sensitivity of 500mV/lb and weighs 0.80oz. A PCB accelerometer (model 353B15) was used to measure the response of the structure. The input and output signals were obtained using two methods. The first method used the force sensor reading as the input signal while the accelerometer reading was used as the output. For the second method, a second PCB accelerometer was attached near the position of the force sensor, and its reading was used as the input, the output signal remained as before. Force sensor and accelerometer placement locations are shown in Figure 12 below while Figure 13 shows a schematic of the initial measurement setup.

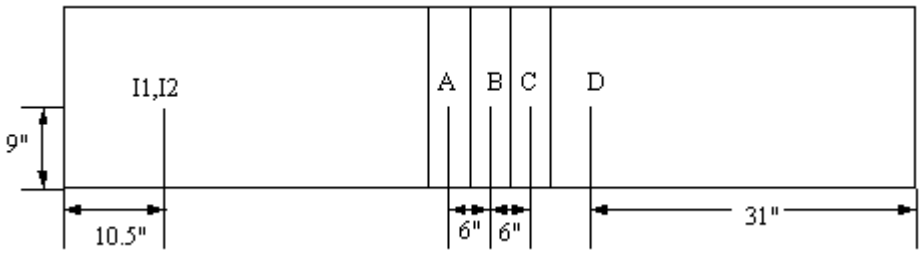

Figure 12. Schematic of sensor locations. Force sensor location: I1 Accelerometer locations A, B, C, D, I2

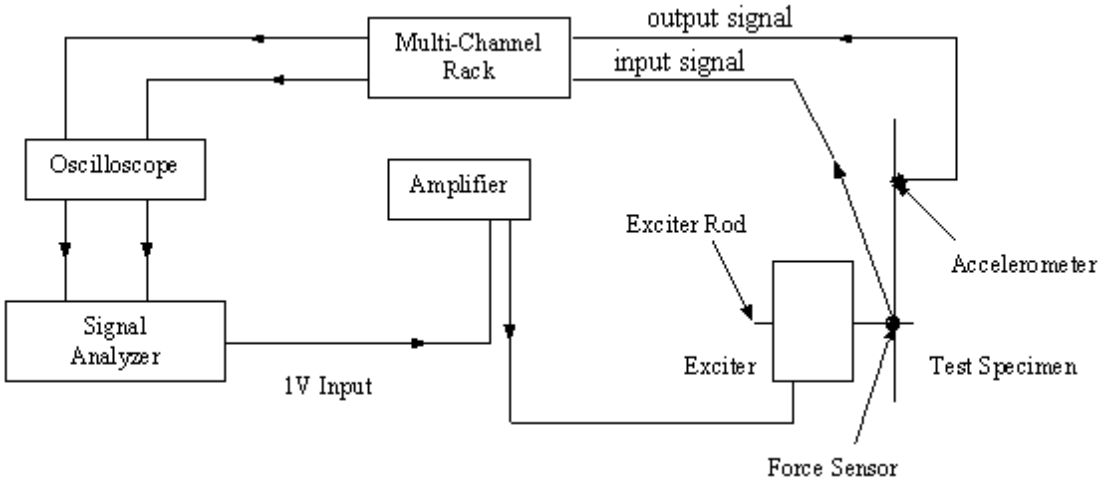

Figure 13. MB Dynamics Modal 50 Exciter Setup

Figure 14 show how the test structures were suspended and attached to the exciter. The test structure was suspended using bungee cords to simulate a free hanging structure.

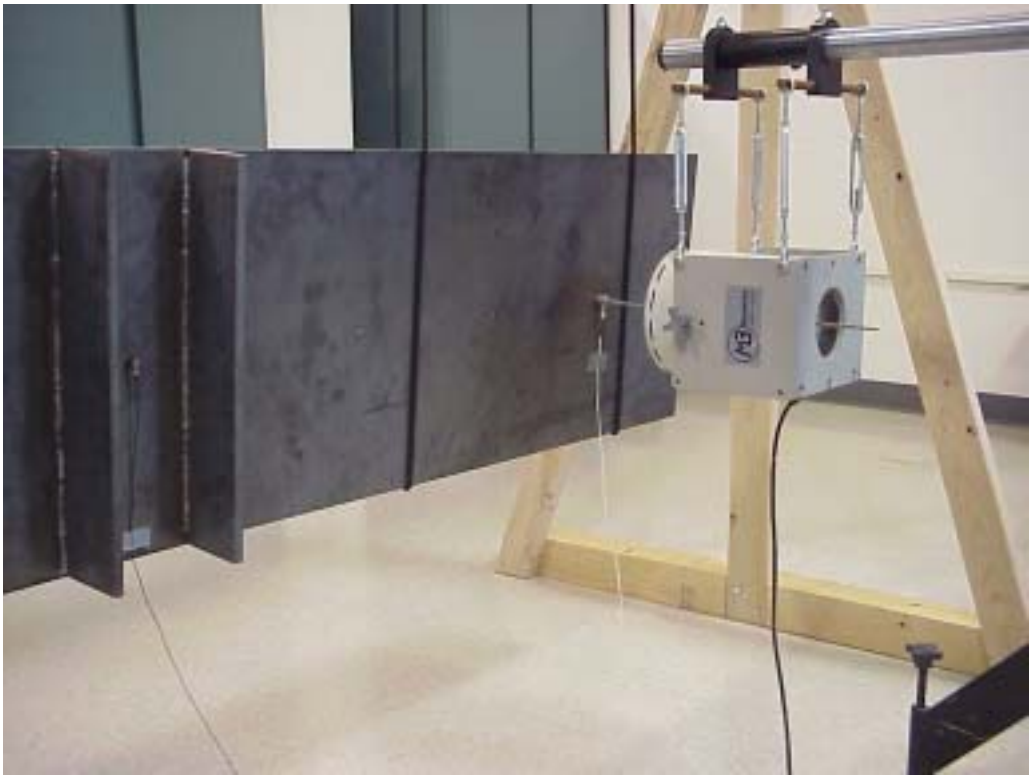

Figure 14. Modal 50 Exciter and Test Structure Setup

During testing, the noise level increased as the accelerometer location moved further from the input location (towards location D), saturating and rendering the output signal at location D useless. To overcome this, the end furthest away from the exciter location was placed in a cardboard box filled with sand. The sand was used in order to dissipate the waveform created by the exciter and preventing it from reflecting back towards the exciter, therefore decreasing the noise level. Figure 15 shows how one of the ends of the test structure was supported using a box filled with sand. For this setup, two other accelerometer locations were used to measure the output signal. These new locations (marked E and F) are shown in Figure 16.

Figure 15. Test structure setup using cardboard box and sand

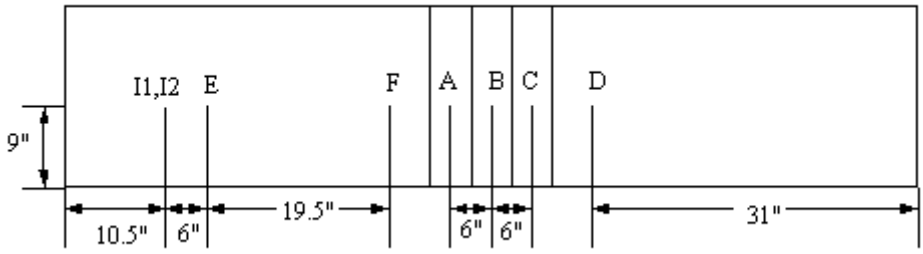

Figure 16. Schematic of sensor locations. Force sensor location: I1 Accelerometer locations A, B, C, D, E, F, I2

B. NUMERICAL SIMULATIONS

In an attempt to relate damping with the mode shape and natural frequency a finite element model was created for each of the structures. All the structures were modeled using quad four shell elements utilizing the MSC Patran/Nastran computer modeling systems. Table 3 lists the number of shell elements used for each of the models. No attempt was made to simulate the actual weld of the structure, two surfaces were simply merged together using the equivalence command in Patran.

Table 3. Number of Shell Elements Used for Each Structure

Structure	Number of Shell Elements
18- inch flat plate	576
18-inch stiffened plate	864
8.5-foot flat plate	7585
8.5-foot stiffened plate	8352

THIS PAGE INTENTIONALLY LEFT BLANK

IV. RESULTS AND DISCUSSION

The tests used to determine the frequency response of the structures were the impact testing, shaker testing, and exciter testing. The natural frequencies were determined using the Nyquist and phase plots of each structure. A zoom measurement of each resonance peak was taken and the damping ratio determined using the half-power point method. One of the objectives when conducting the experimental testing was to obtain a coherence of unity. The coherence provides a non-dimensional measure of the linear dependence between the input and output signals. It is a measure of the power in the output signal caused by the input signal, so a coherency of 1 shows that all the power of the output signal is caused by the input signal and there is little to no noise cluttering the signal. It is an indication of the statistical validity of the frequency response measurement [10].

A. IMPACT TESTING

The impact testing was used to determine the frequency response of the small flat plate, welded stiffened plate, and machined stiffened plate. Each specimen was supported using two bungee chords. The structure was impacted at the lower left end of the structure and the response was measured at arbitrary locations on the opposite side of the plate. The dynamic signal analyzer recorded the stable mean of 20 impacts for each plate. The problem encountered during testing was that the coherence measurement never reached unity. This can be attributed to the output signal being saturated by a significant amount of noise. Figure 17 shows a typical coherence plot obtained during testing. The data obtained during the impact testing was therefore determined useless and the impact testing was abandoned for the shaker testing.

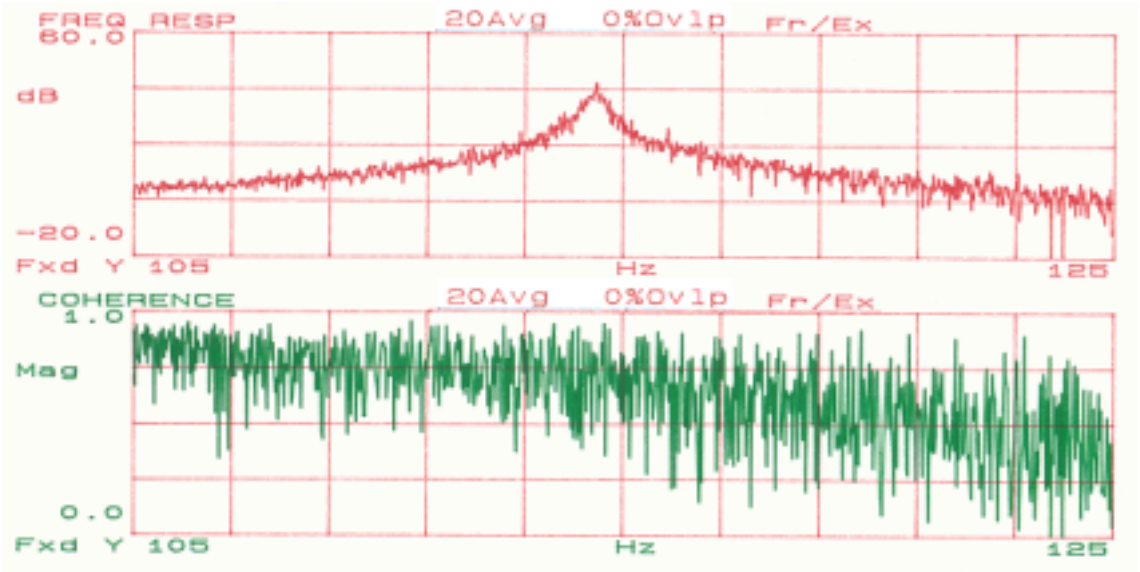

Figure 17. Typical coherence response obtained during testing of flat plate, welded stiffened plate, and machined stiffened plate

B. SHAKER TESTING

The shaker testing was used to determine the frequency response of the small flat plate, welded stiffened plate, and machined stiffened plate. A small hole was drilled off-center on each plate and attached to the generator using a threaded stud and nut, while the ends were supported by bungee cords. The input and output signals were determined by two methods. The first method was to use the force gage located in the generator as the input and the accelerometer located in the generator as the output. The second method was to use the accelerometer in the generator as the input and a PCB accelerometer (model 303A03), located at two random points as the output.

1. Flat Plate

For the initial testing, the force gage and accelerometer located in the shaker were used as the input and output, respectively. A 1V random noise signal was used as the input for the generator. The test was conducted for a frequency range of 2 to 1100 Hz and analyzed with 35 averages. Figure 18 is a sample frequency plot of the flat plate determined using the Wilcoxon F4/F7 generator with the input and output at the generator. The next step was to calculate the damping ratios using a zoom measurement of the resonance peak by isolating the natural frequencies in a frequency band that would

capture the correct characteristics of the peak. Figure 19 is an example of a resonance peak used to determine the damping ratio associated with each natural frequency

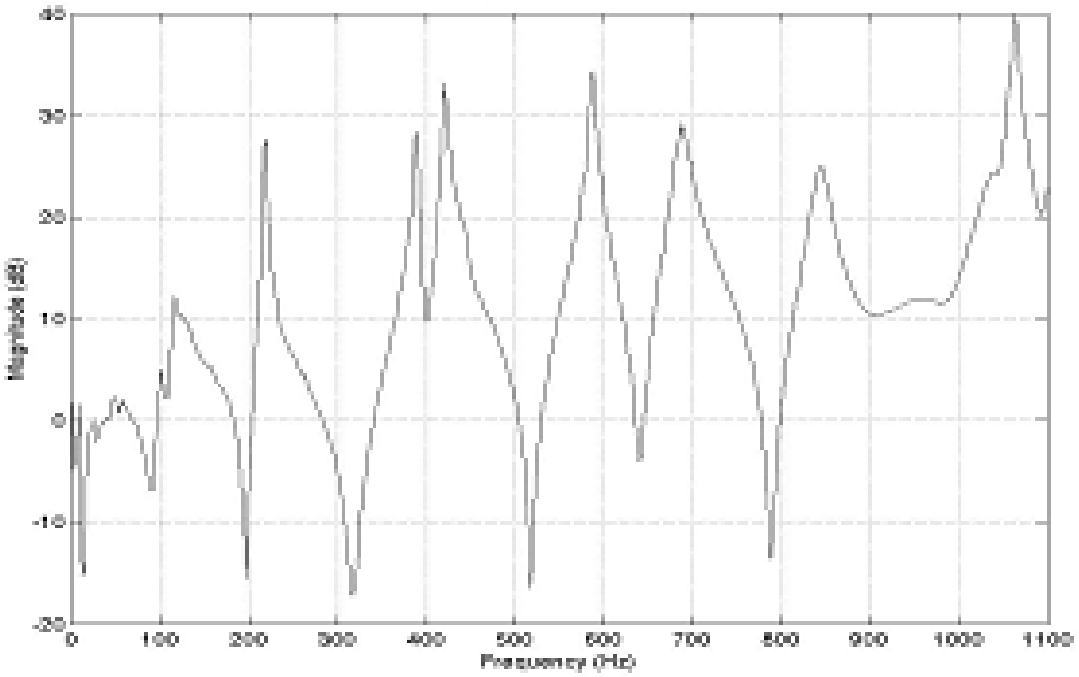

Figure 18. Sample frequency response of flat plate, input and output measured at the generator

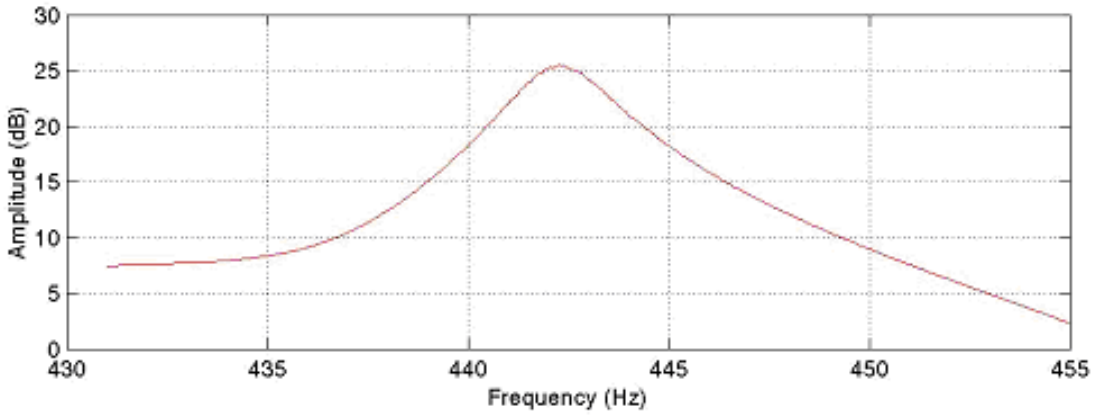

Figure 19. Sample resonance peak used to determine damping ratio

The damping ratio for six randomly chosen natural frequencies was determined using the half-power point method and results are shown in Table 4.

Table 4. Natural frequencies and associated damping ratios for flat plate. Force gage and accelerometer on generator used as input and output, respectively

ω_n (Hz)	ζ (%)
247	0.37
443	0.21
482.3	0.24
675	1.28
1214.2	0.14

For the second round of testing, the accelerometer in the generator was used as the input and an external accelerometer located at two random locations was used as the output. The two random locations are shown in Figure 8. Again the frequency response was analyzed and damping ratios calculated. Table 5 shows the results.

Table 5. Natural frequencies and associated damping ratios for flat plate. Force gage on generator used as input, external accelerometer used as output

Location A		Location B	
ω_n (Hz)	ζ (%)	ω_n (Hz)	ζ (%)
226.6	0.94	226.3	1.105
361	0.65	361.5	0.69
590.8	0.48	457.8	1.12
731.9	1.02	590.5	0.38
887.5	0.27	899	0.17

As can be seen from Tables 4 and 5, some of the natural frequencies are fairly similar but others are different for each of the three locations. This may be attributed to the fact that the accelerometer measured the output at different locations and it picked up different modes of the structure.

2. Welded Stiffened Plate

The same test procedure used for the flat plat was used for the welded stiffened plate. Figure 20 shows the frequency responses measured at location A for the welded stiffened plate. Table 6 shows the natural frequencies and damping ratios calculated for each of the three measured locations.

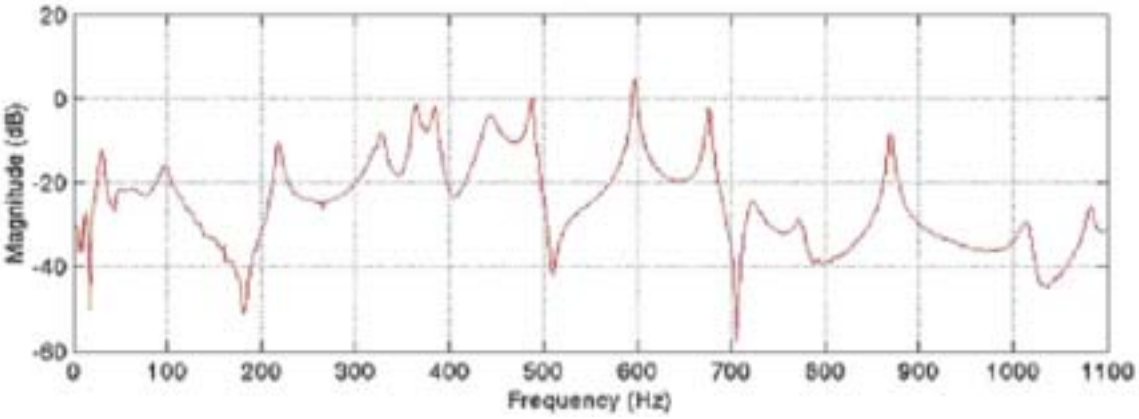

Figure 20. Sample frequency response of welded stiffened plate. Accelerometer on generator used as input, external accelerometer positioned at location A used as output

Table 6. Natural frequencies and associated damping ratios for welded stiffened plate for the three different measurement locations.

Shaker		Location A		Location B	
ω_n (Hz)	ζ (%)	ω_n (Hz)	ζ (%)	ω_n (Hz)	ζ (%)
386.8	0.68	245.8	1.14	246.2	1.14
456	1.68	370.8	1.46	-	-
537.8	1.02	552.9	0.36	553.7	0.36
723.5	1.4	677	0.19	677.4	0.19
968.6	0.8	767	0.23	818.4	1.2

As before, the natural frequencies are not the same for each point, again due to the fact that the accelerometer measured the output at different locations, therefore picking up different modes of the structure.

3. Machined Stiffened Plate

Using the same procedure as above, the frequency response and damping ratios were determined for the machined stiffened plate. Figure 21 shows the frequency response measured at location A of the machined stiffened plate. Table 7 shows the natural frequencies and damping ratios calculated at each of the three measured locations.

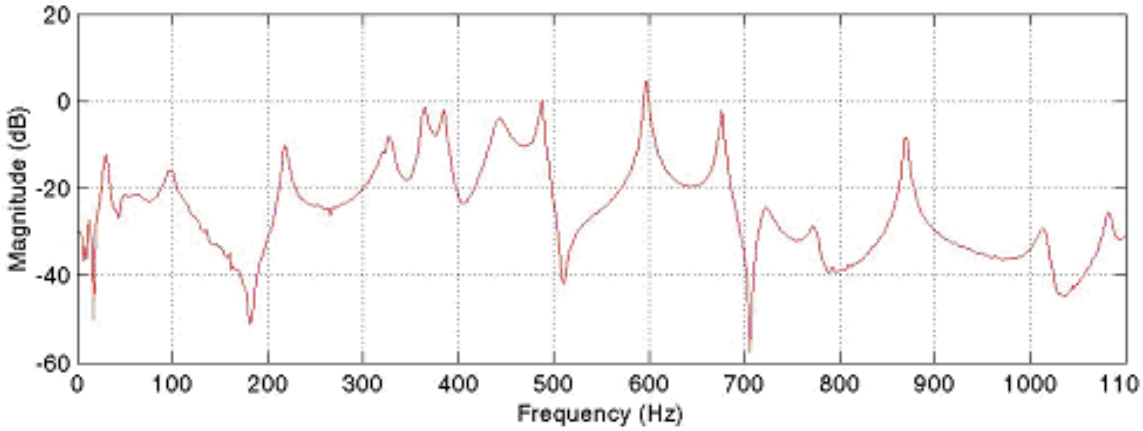

Figure 21. Sample frequency response of machined stiffened plate. Accelerometer on generator used as input, external accelerometer positioned at location A used as output

Table 7. Natural frequencies and associated damping ratios for welded stiffened plate for the three different measurement locations

Shaker		Location A		Location B	
ω_n (Hz)	ζ (%)	ω_n (Hz)	ζ (%)	ω_n (Hz)	ζ (%)
-	-	141.3	2.27	142.5	3.12
536.9	0.57	327.3	0.68	327.1	0.69
611.4	0.33	557.5	0.51	392.5	0.85
763.5	0.58	629	0.56	556.9	0.51
820.4	0.4	794.6	0.45	629.7	0.62

C. EXCITER TESTING

The exciter testing was used to determine the frequency response of the 8.5-foot flat plate and welded stiffened plate. A small hole was drilled at one end of the plate and the exciter force was transmitted to the structure via a 10-32 stainless steel threaded rod attached to a PCB force sensor (model 208C01) and bolted to the structure, the structure was supported by bungee cords. The input and output signals were determined by two methods. The first method used the force sensor reading as the input signal while the accelerometer reading was used as the output. For the second method, a second PCB accelerometer was attached near the position of the force sensor, and it's reading was used as the input, the output signal remained as before.

1. Flat Plate

For the initial testing, the readings from a force sensor positioned at location I1 were used as the input signal and the readings from an accelerometer positioned at several locations were used as the output signal. A 500 mV random noise signal was used as the input for the exciter. The test was conducted for a frequency range of 2 to 1100 Hz and analyzed with 35 averages. Figure 22 is a sample frequency plot of the flat plate determined using the MB Dynamics exciter with the force sensor used as the input and the output at location C.

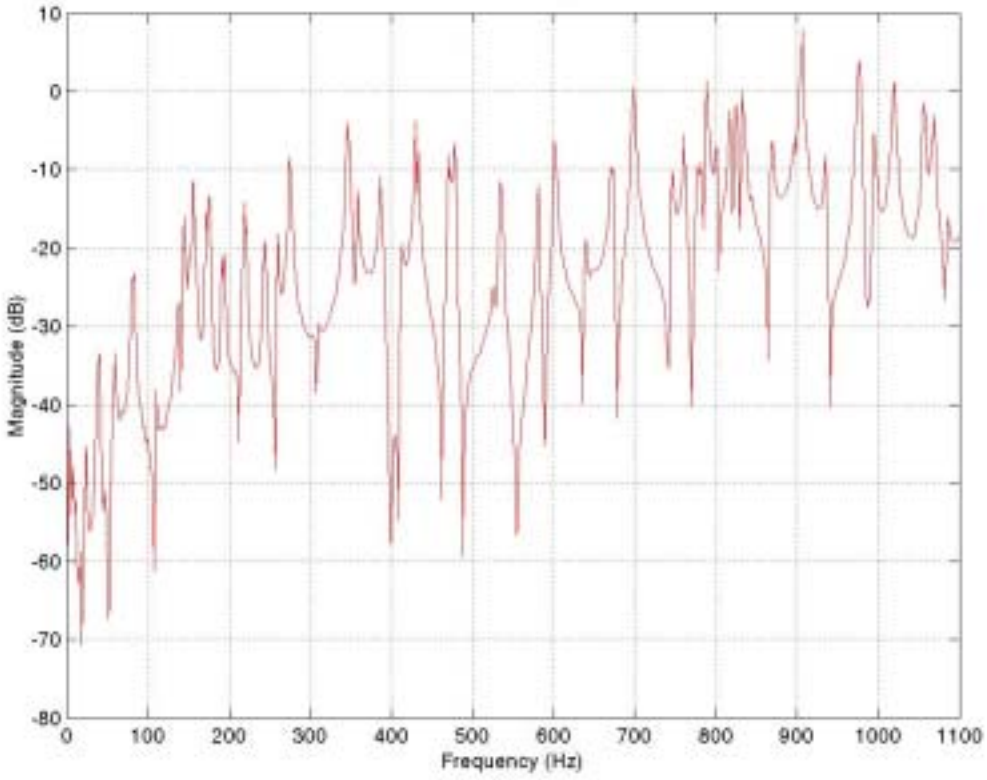

Figure 22. Frequency response of 8.5-foot flat plate using MB Dynamics exciter with force sensor uses as the input and output at location C

Using the frequency plot, the natural frequencies were determined along with the damping ratios. Table 8 shows the natural frequencies and damping ratios determined for locations A, B, C. At location D, noise saturated the output signal and prevented the calculation of the natural frequencies and damping ratios.

Table 8. Natural frequencies and damping ratios determined for the 8.5-foot flat plate using MB Dynamics exciter, force sensor at location I1 used as input

Location A		Location B		Location C	
ω_n (Hz)	ζ (%)	ω_n (Hz)	ζ (%)	ω_n (Hz)	ζ (%)
177.9	0.056	177.9	0.039	177.9	0.037
312.8	0.038	351.9	0.024	489.9	0.04
490.1	0.025	440.2	0.037	684.2	0.048
684.2	0.037	684.2	0.054	794.8	0.057
794.5	0.05	794.5	0.053	897.5	0.045
1030.7	0.029	939	0.035	1030.3	0.046

For the second run of tests, an accelerometer was placed at position I2 and used as the input signal; the output signals remained as before. Figure 23 shows a frequency plot for the flat plate with the output measured at location C. Once again, the natural frequencies and associated damping ratios were determined. Table 9 shows the results.

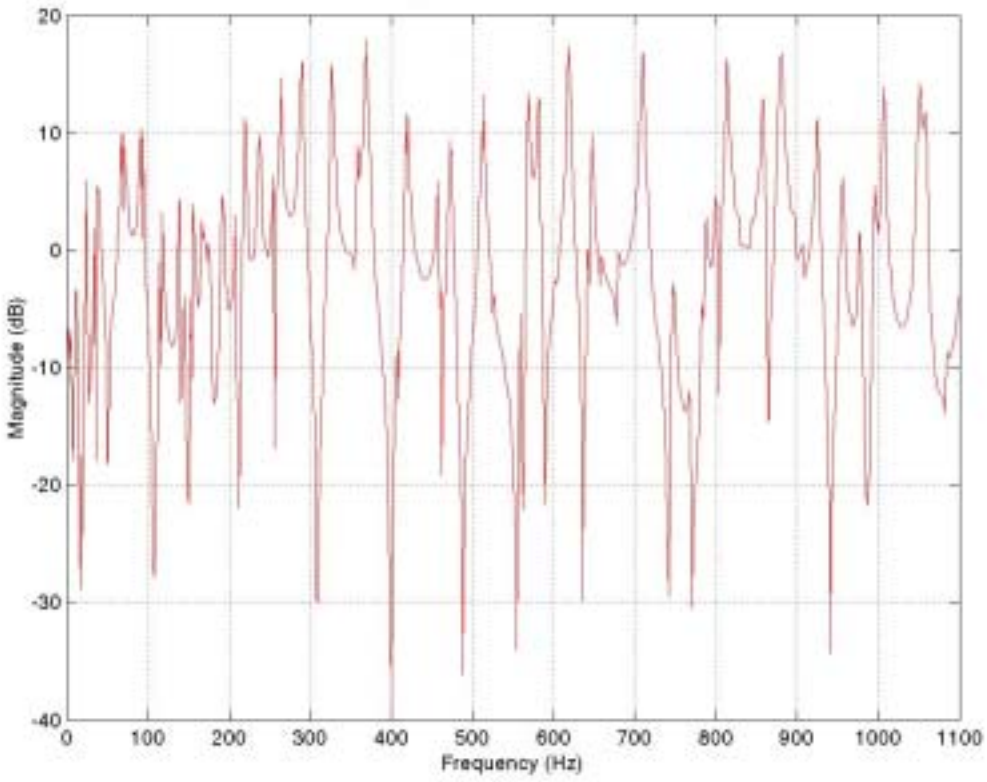

Figure 23. Frequency response of flat plate using MB Dynamics exciter with accelerometer at location I1 as the input and output at location C

Table 9. Natural frequencies and damping ratios determined for 8.5-foot flat plate using the MB Dynamics exciter, accelerometer readings located at I2 used as input

Location A		Location B		Location C	
ω_n (Hz)	ζ (%)	ω_n (Hz)	ζ (%)	ω_n (Hz)	ζ (%)
329	0.061	217.3	0.048	328.9	0.053
583.8	0.043	420	0.077	419.9	0.059
703.8	0.039	537.9	0.037	583.2	0.051
803.4	0.036	807.6	0.074	807.3	0.077
976.4	0.051	976.5	0.043	925.6	0.049
1091.5	0.025	1091.7	0.027	1001.5	0.065

To overcome the noise saturation at locations further away from the excitation point, that end of the plate was inserted into a sand-filled box, in an attempt to absorb the excitation wave and prevent it from transmitting back toward the excitation point. Figure 24 shows the frequency response of the 8.5-foot flat plate with one of its ends inserted in sand, the measurement was taken at location C. Table 10 shows the natural frequencies and associated damping ratios for this configuration.

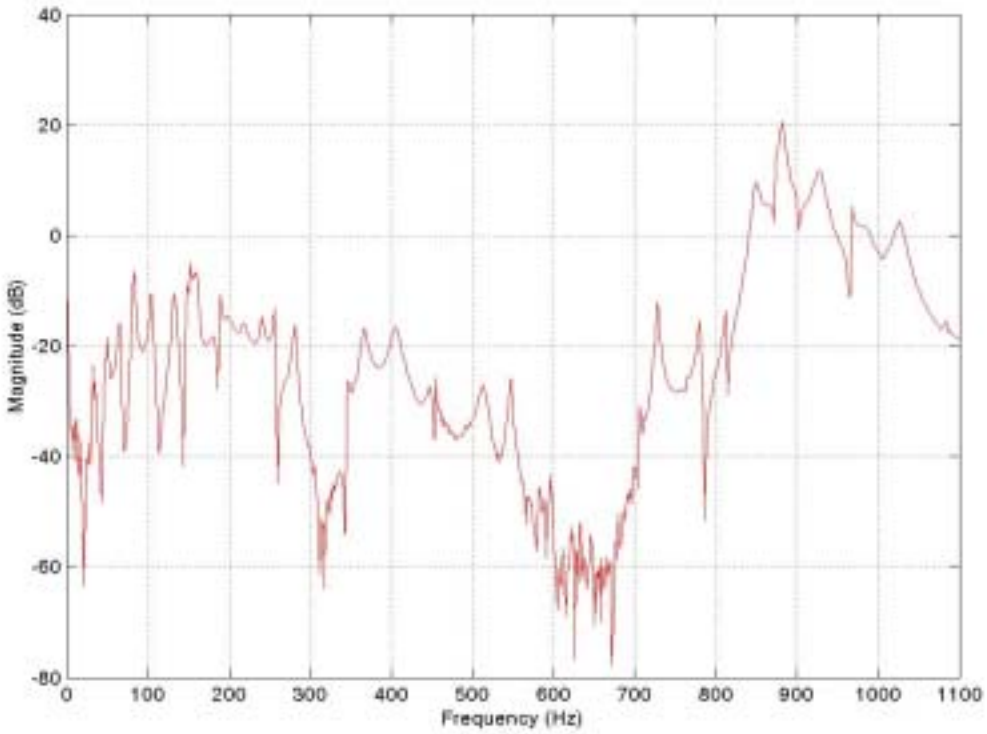

Figure 24. Frequency response of 8.5-foot plate inserted in sand with force sensor at location I1 as the input and output at location C

Table 10. Natural frequencies and damping ratios determined for 8.5-foot flat plate with one end inserted into sand

Location A		Location B		Location C	
ω_n (Hz)	ζ (%)	ω_n (Hz)	ζ (%)	ω_n (Hz)	ζ (%)
165.6	0.544	165.7	0.604	166.2	0.631
388.5	1.29	-	-	389.6	1.38
485.2	1.39	484.7	1.65	486.2	1.48
Location D		**Location E**		**Location F**	
165.8	0.543	166.8	0.51	165.8	0.543
390	2.17	389	1.47	390	2.17
486.2	0.617	485.1	1.19	486.2	0.617

For the testing with the plate inserted in sand, only natural frequencies below 500Hz were used because the damping is higher at these lower frequencies. An attempt was made to pick up the same natural frequencies at all locations. As can be seen from the results in Tables 9 and 10, the damping ratio increased when the plate was inserted in sand, this

increase can be attributed to the sand. But the increase in damping can be assumed to be the same for both plates so the trend of the change in damping can be observed.

2. Stiffened Plate

The same procedure used for the 8.5-foot flat plate was used on the 8.5-foot stiffened plate to determine the natural frequencies and damping ratios. Figure 25 show the frequency response plot for the 8.5-foot stiffened plate using the force sensor as the input and the transducer located at location C as the output. Table 11 summarizes the natural frequencies and associated damping ratios determined using the force sensor readings as the input and the accelerometer readings as the output.

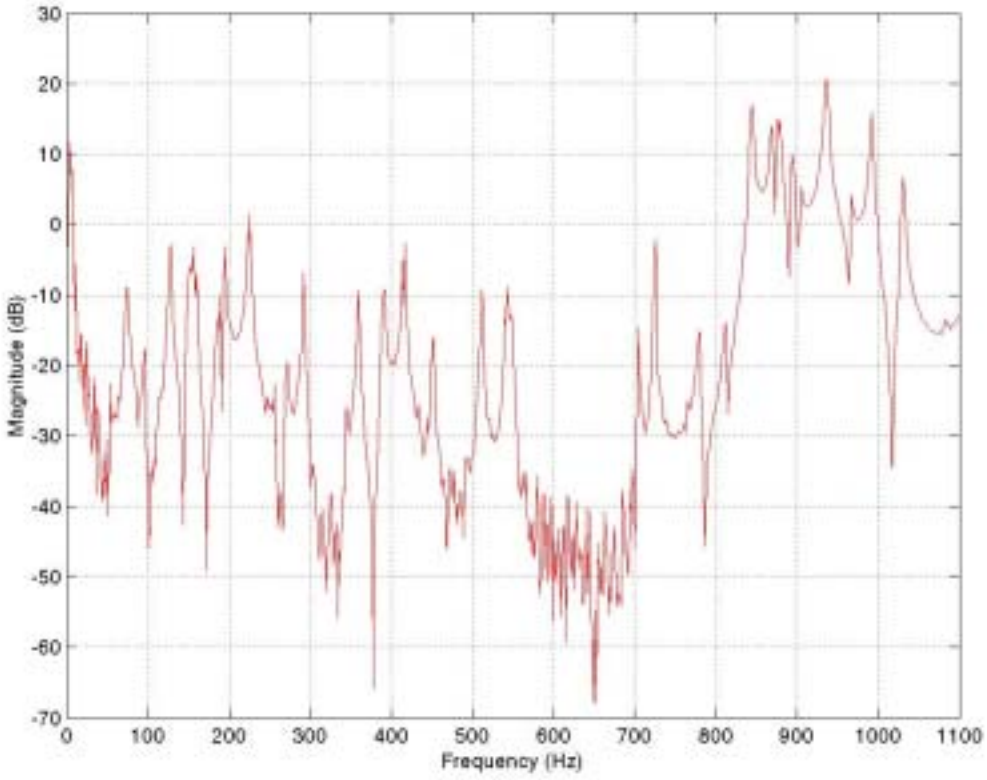

Figure 25. Frequency response of 8.5-foot stiffened plate with force sensor at location I1 as the input and accelerometer at location C as the output.

Table 11. Natural frequencies and damping ratios determined for 8.5-foot stiffened plate. Force sensor readings used as the input and the accelerometer readings used as the output

Location A		Location B		Location C	
ω_n (Hz)	ζ (%)	ω_n (Hz)	ζ (%)	ω_n (Hz)	ζ (%)
144.2	0.031	110.7	0.036	179.6	0.047
255	0.027	255	0.024	255	0.029
331.6	0.02	331.6	0.02	331.7	0.021
515.4	0.073	512.3	0.043	581	0.04
826.9	0.022	827.2	0.054	824.1	0.03
1064.7	0.045	1015.5	0.079	-	-

Figure 26 shows the frequency response of the 8.5-foot stiffened plate using the accelerometer readings at location I2 as the input and the accelerometer readings at location C as the output. Table 12 shows the natural frequencies and associated damping ratios obtained using the accelerometer readings as the input and output.

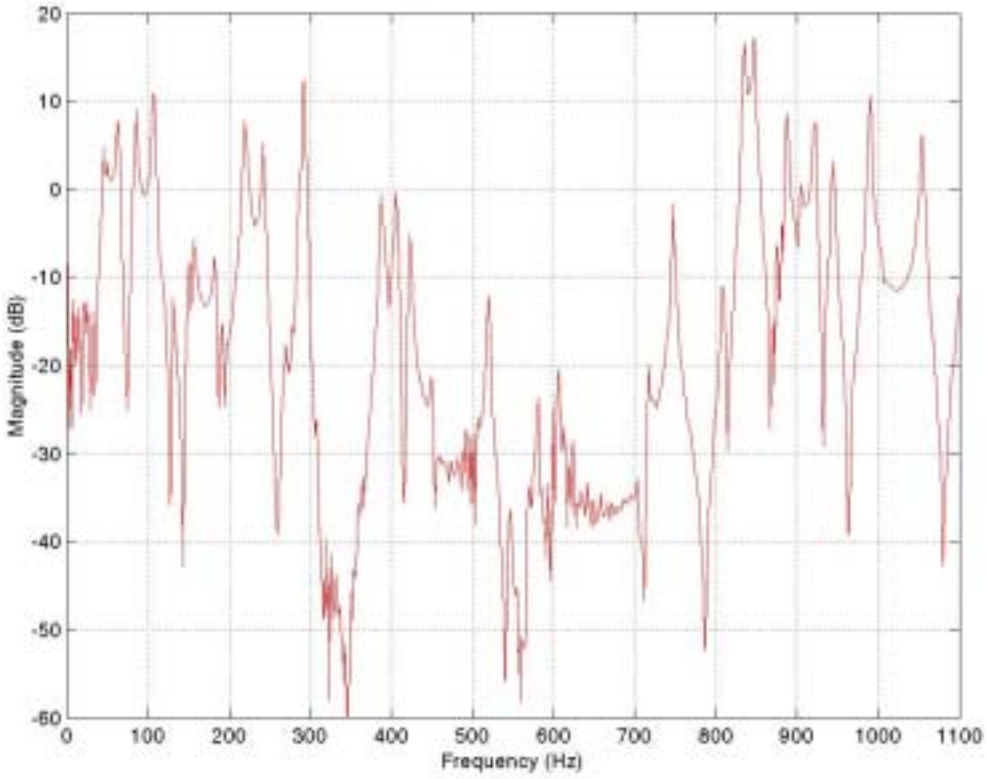

Figure 26. Frequency response of 8.5-foot stiffened plate with accelerometer at location I1 as the input and accelerometer at location C as the output.

Table 12. Natural frequencies and damping ratios determined for 8.5-foot stiffened plate. Accelerometer readings used as input and output signals.

Location A		Location B		Location C	
ω_n (Hz)	ζ (%)	ω_n (Hz)	ζ (%)	ω_n (Hz)	ζ (%)
-	-	249.7	0.034	249.1	0.185
208.6	0.072	329.1	0.058	329.1	0.16
477.5	0.073	479.85	0.052	461.8	0.087
661	0.043	591.4	0.093	591.9	0.063
850.2	0.034	850.2	0.064	850.1	0.047
1048.6	0.02	1049	0.043	1049.3	0.029

Figure 27 shows the frequency response of the 8.5-foot stiffened plate with one of its ends inserted in sand, the measurement was taken at location C. Table 13 shows the natural frequencies and associated damping ratios for this configuration.

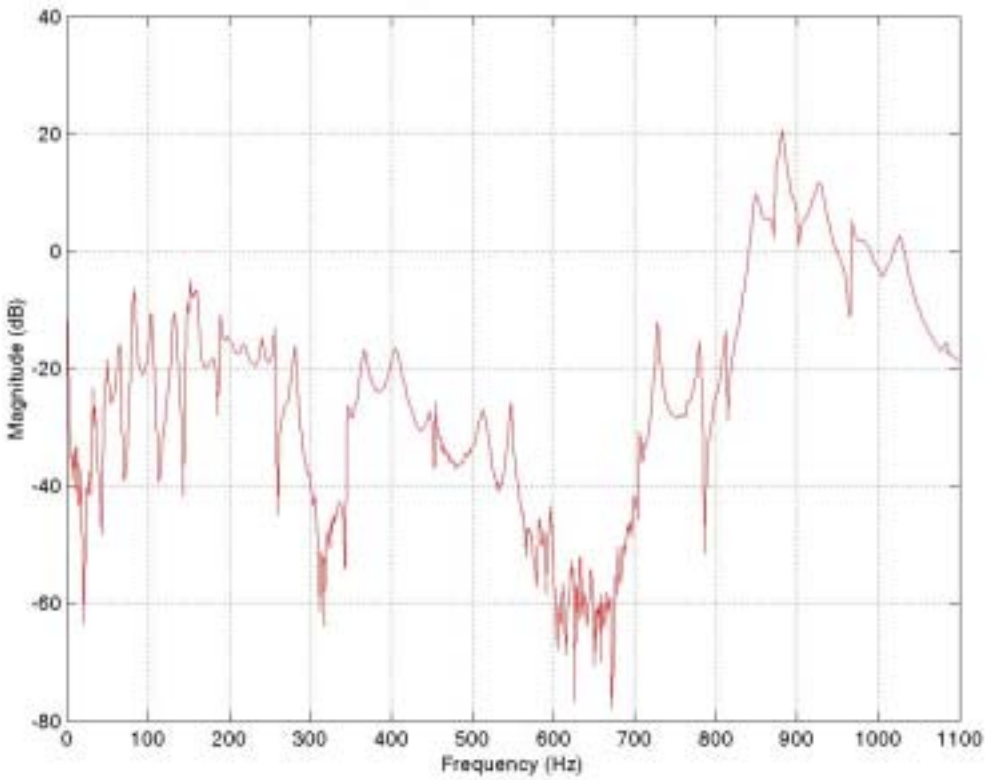

Figure 27. Frequency response of 8.5-foot stiffened plate inserted in sand with force sensor at location I1 as the input and output at location C

Table 13. Natural frequencies and damping ratios determined for 8.5-foot stiffened plate with one end inserted into sand

Location A		Location B		Location C	
ω_n (Hz)	ζ (%)	ω_n (Hz)	ζ (%)	ω_n (Hz)	ζ (%)
150.8	1.13	150.2	1.16	150.9	1.09
292	0.039	291.9	0.036	291.9	0.034
321.3	0.521	321.3	0.521	320.9	0.436
Location D		Location E		Location F	
150.6	1.13	150.5	1.05	150.5	1.1
291.9	0.034	291.8	0.033	291.9	0.036
321.4	0.482	320.6	0.438	-	-

D. NUMERICAL RESULTS

Utilizing the MSC Patran/Nastran modeling systems, a finite element model was developed for each of the structures. The attempt was to observe trends that would relate the mode shape of a structure with damping and natural frequency. Table 14 shows the natural frequencies and mode shape numbers obtained using the finite element model that matched the experimental results along with the experimental damping ratio.

Table 14. Natural frequencies and mode shapes for each test structures

Structure	Numerical ω_n (Hz)	Experimental ω_n (Hz)	Mode Shape #	ζ (%)
18-inch flat plate	236.2	226.6	4	1.02
	392.3	361	5	0.67
18-inch stiffened plate	266.1	245.8	2	1.14
	372.1	370.8	4	1.46
8.5-foot flat plate	124.5	150.8	6	1.11
	268.2	292	10	.035
	351.2	321.3	12	0.47

Figures 28, 29 and 30 show the mode shapes of each of the structures. The mode shapes shown are associated with the numerical frequencies that matched the experimental frequencies.

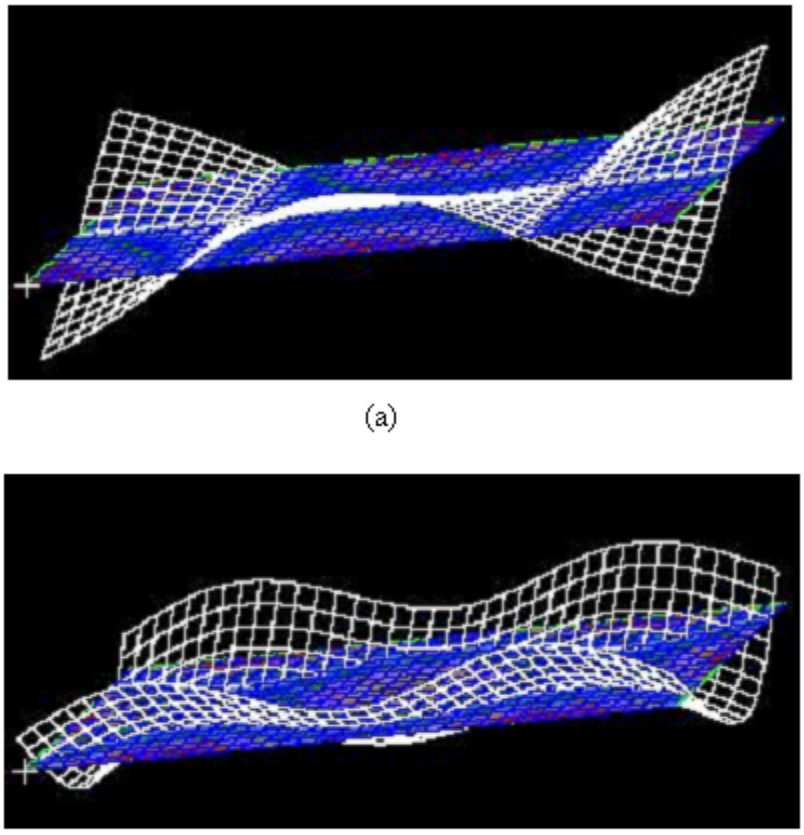

Figure 28. Mode shapes for 18-inch flat plate (a) 4th mode shape (b) 5th mode shape

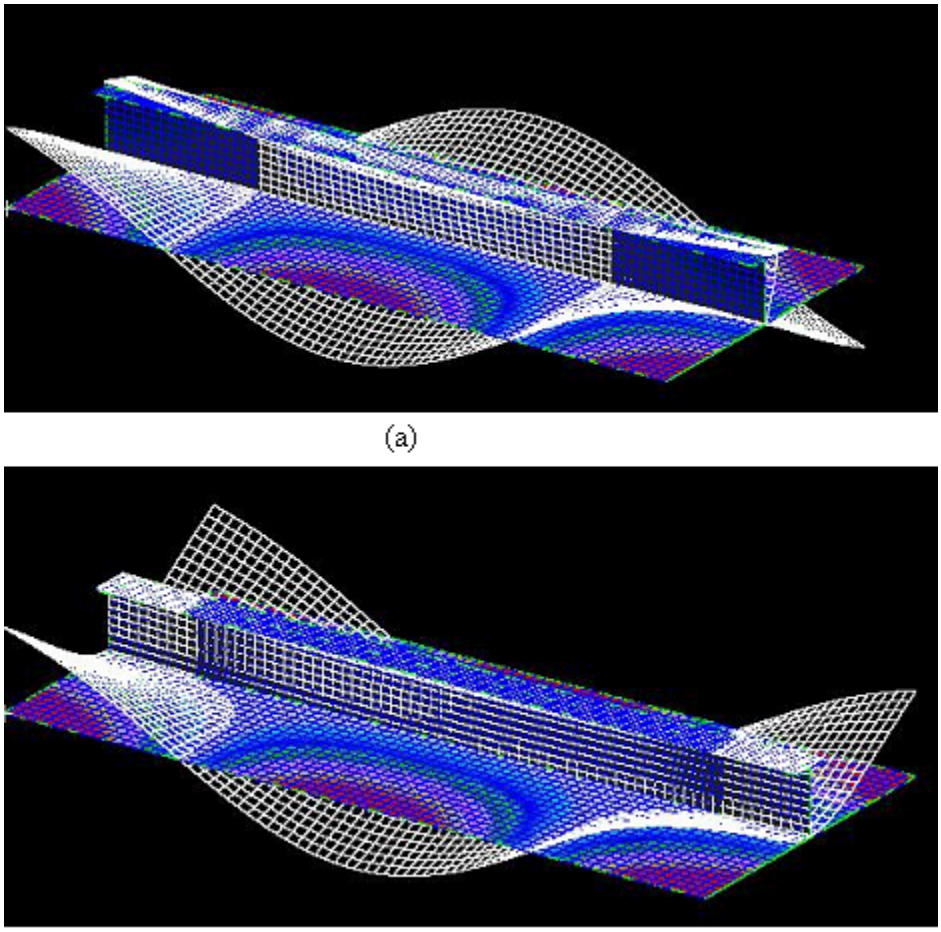

Figure 29. Mode shapes for 18-inch stiffened plate (a) 2nd mode shape (b) 4th mode shape

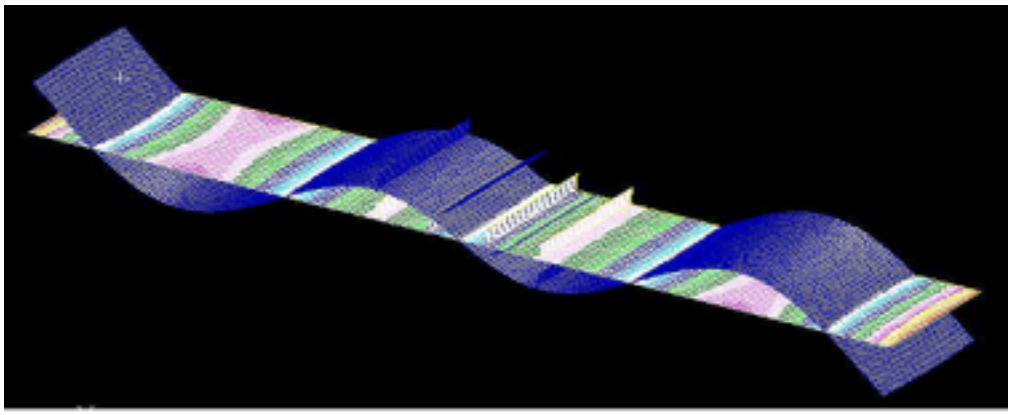

(a)

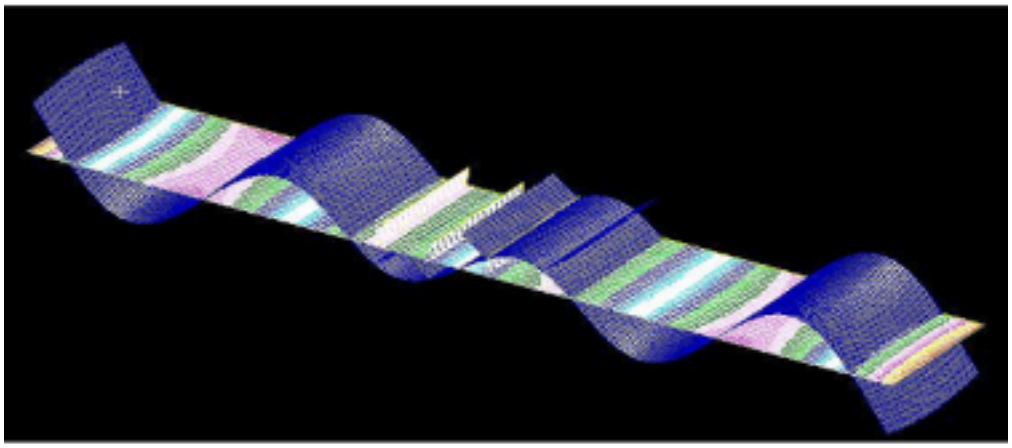

(b)

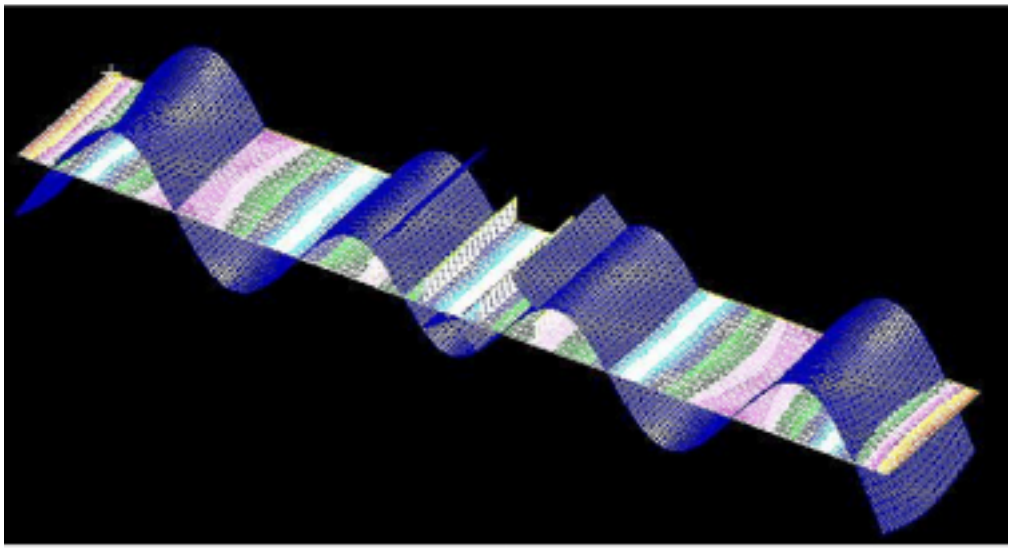

(c)

Figure 30. Mode shapes of 8.5-foot stiffened plate (a) 6th mode shape (b) 10th mode shape (c) 12th mode shape

One observation that can be made from the results of Table 14 and Figures 29, 29 and 30, at the mode shape that experiences the higher degree of stress at the weld, the damping ratio tends to be higher. Figures 28(a), 29(b) and 30(a) show that at the mode shapes where the weld experiences the highest level of stress, the damping ratio tends to be higher as can be seen in Table 14.

V. TEST COMPARISONS

To get a better grasp of the effects welding has on damping, the damping ratio versus frequency was plotted for each test specimen at each of the measured locations. Figures 31, 32 and 33 compare damping ratios and frequency response for each of the 18-inch plates.

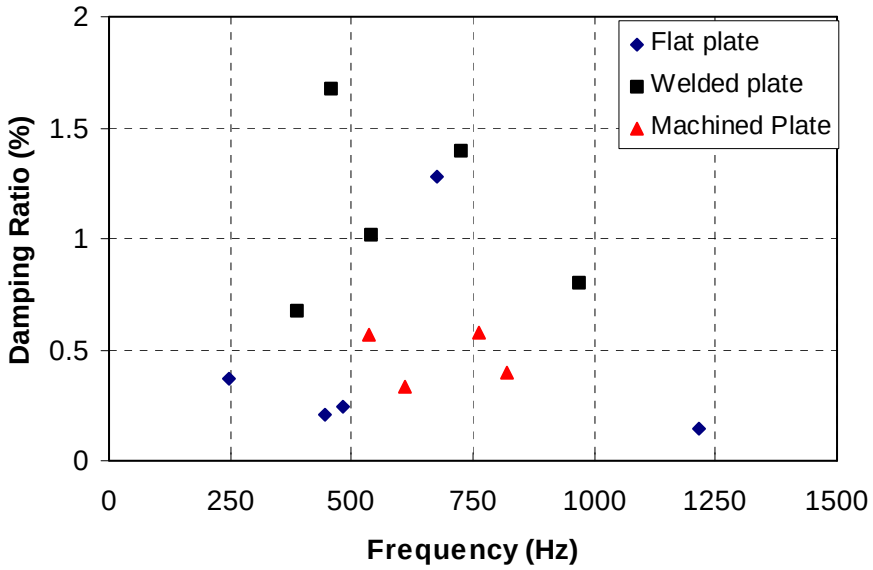

Figure 31. Damping Ratio vs. Frequency response for the flat plate, welded stiffened plated, and machined stiffened plate measured at the shaker.

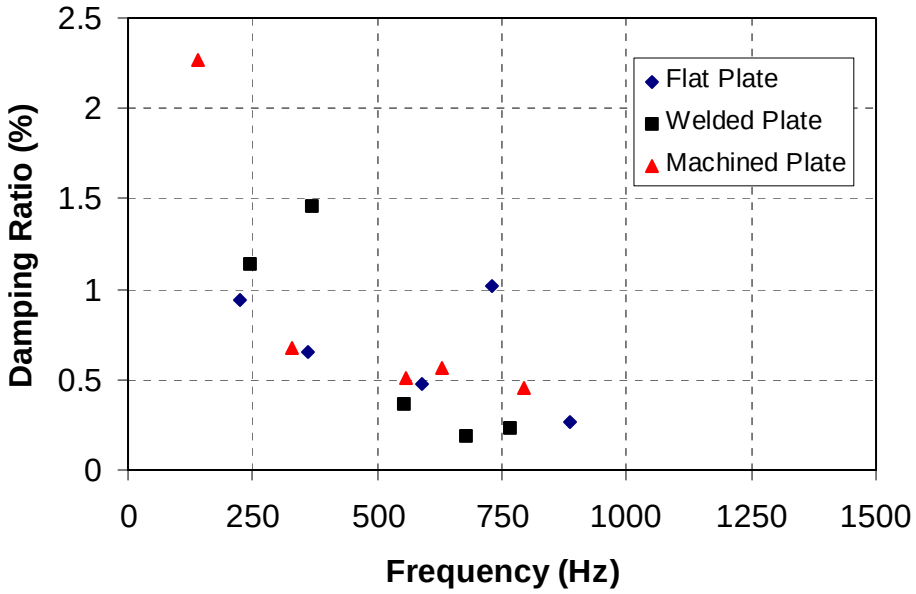

Figure 32. Damping Ratio vs. Frequency response for the flat plate, welded stiffened plated, and machined stiffened plate measured at the location A

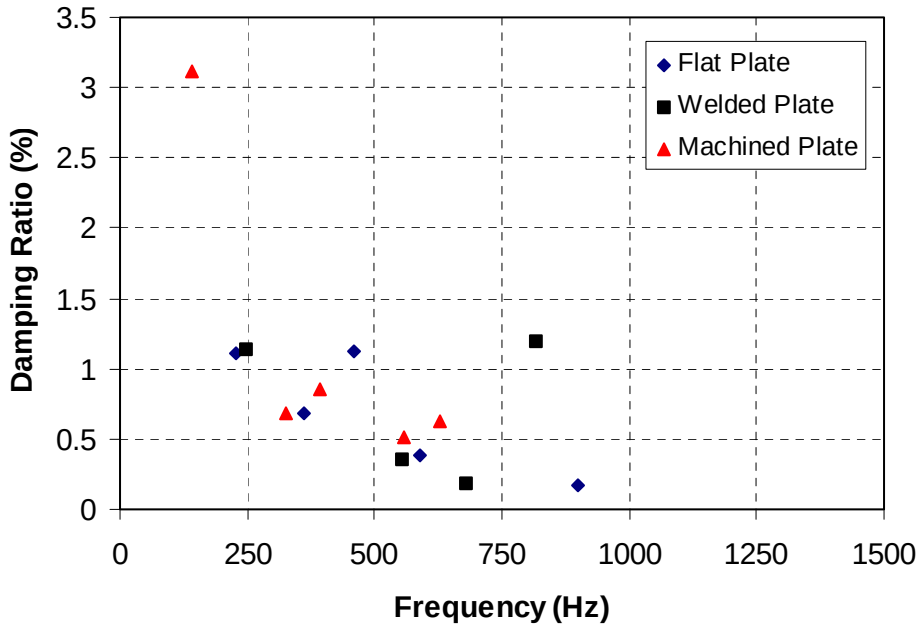

Figure 33. Damping Ratio vs. Frequency response for the flat plate, welded stiffened plated, and machined stiffened plate measured at the location B.

As can be seen in Figures 31, 32 and 33 the damping ratios obtained show a wide degree of scatter. The expectation was that the welded plate would have the higher degree of damping followed by the machined plate and the flat plate. Comparing the results in the figure, at frequencies below 500 Hz and at similar frequencies, the damping of the welded stiffened plate is greater than that of the flat plate and machined stiffened plate. Another expectation was that damping would decrease as the frequency increased, which is the trend shown in Figures 32 and 33, but not Figure 31. Since the frequencies obtained vary widely, an average damping was not able to be determined for each of the natural frequencies. Another observation that can be made from these results is that damping varies greatly within a structure and is difficult to predict.

Figures 34 and 35 compares the damping ratios of the 8.5-foot plates. As can be seen in the figures, the effects of welding on damping are not clear. The expectation was that the stiffened plate would have a higher degree of damping than the flat plate but from Figures 34a and 34c this is not the case. Although the damping ratios for the stiffened plate are higher in some cases, no true evaluation can be made from the results and the data collected simply varied a great deal

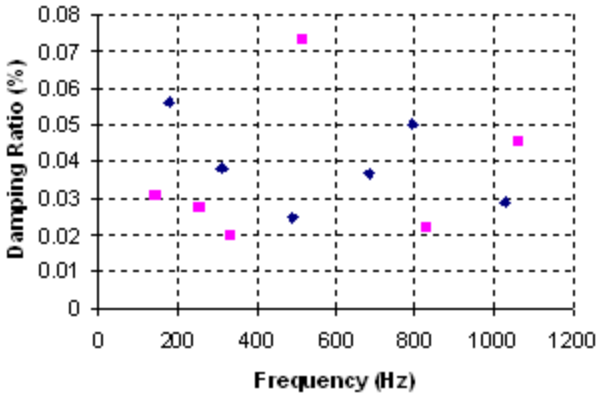

(a)

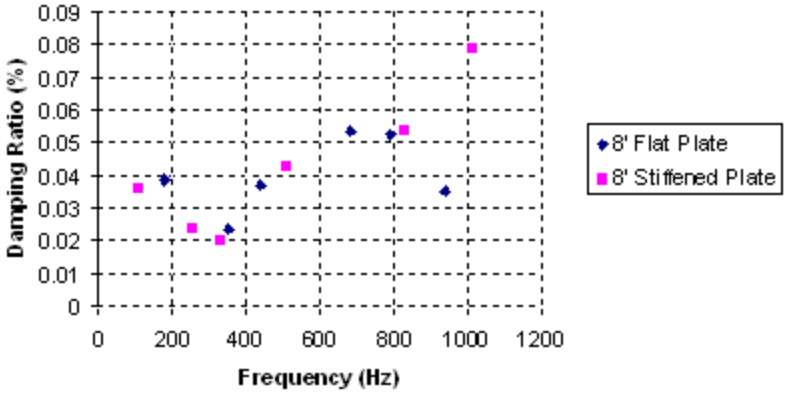

(b)

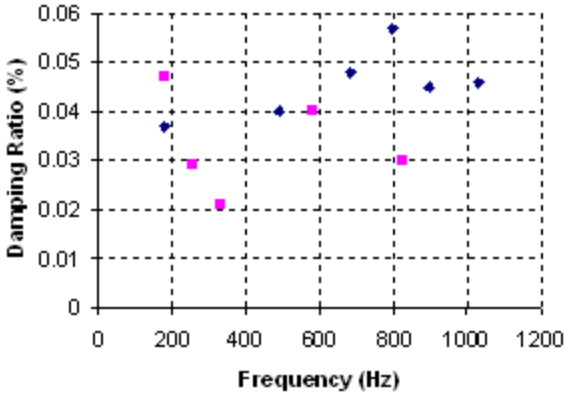

(c)

Figure 34. Damping Ratio vs. Frequency response for 8.5-foot plates using the force sensor as the input signal and the accelerometer as the output signal. (a) measured at location A (b) measured at location B (c) measured at location C

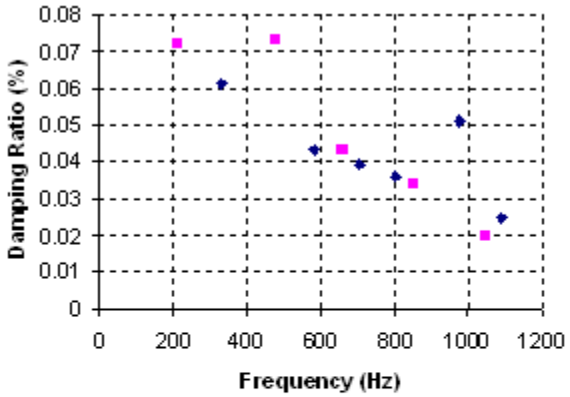

(a)

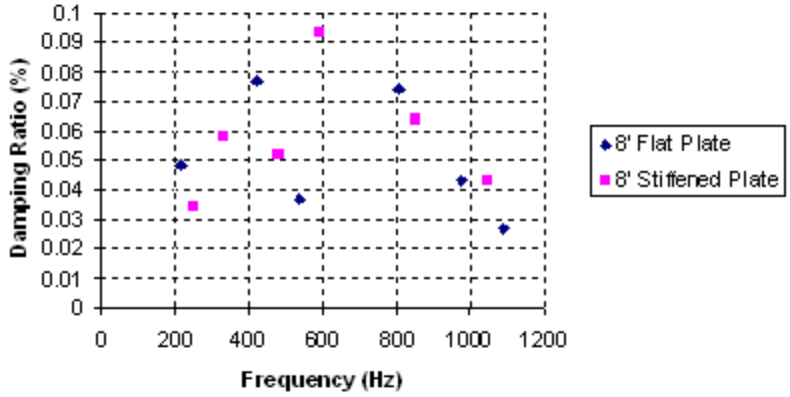

(b)

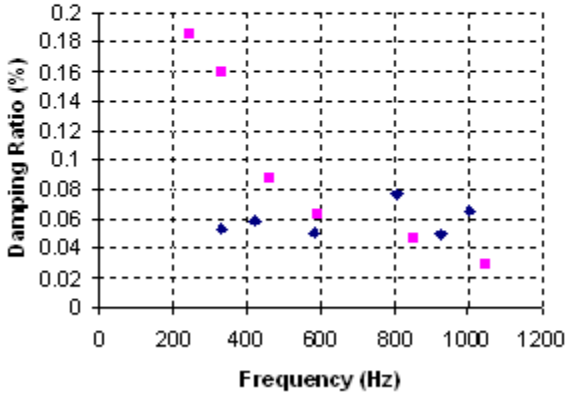

(c)

Figure 35. Damping Ratio vs. Frequency response for 8.5-foot plates using the accelerometers as the input and output signals. (a) measured at location A (b) measured at location B (c) measured at location C

Figure 36 compares the damping ratios of the 8.5-foot plates with one end inserted in sand. As can be seen from the figures, the damping again is widely scattered

but at frequencies below 500 Hz, the stiffened welded plate seem to have a higher degree of damping.

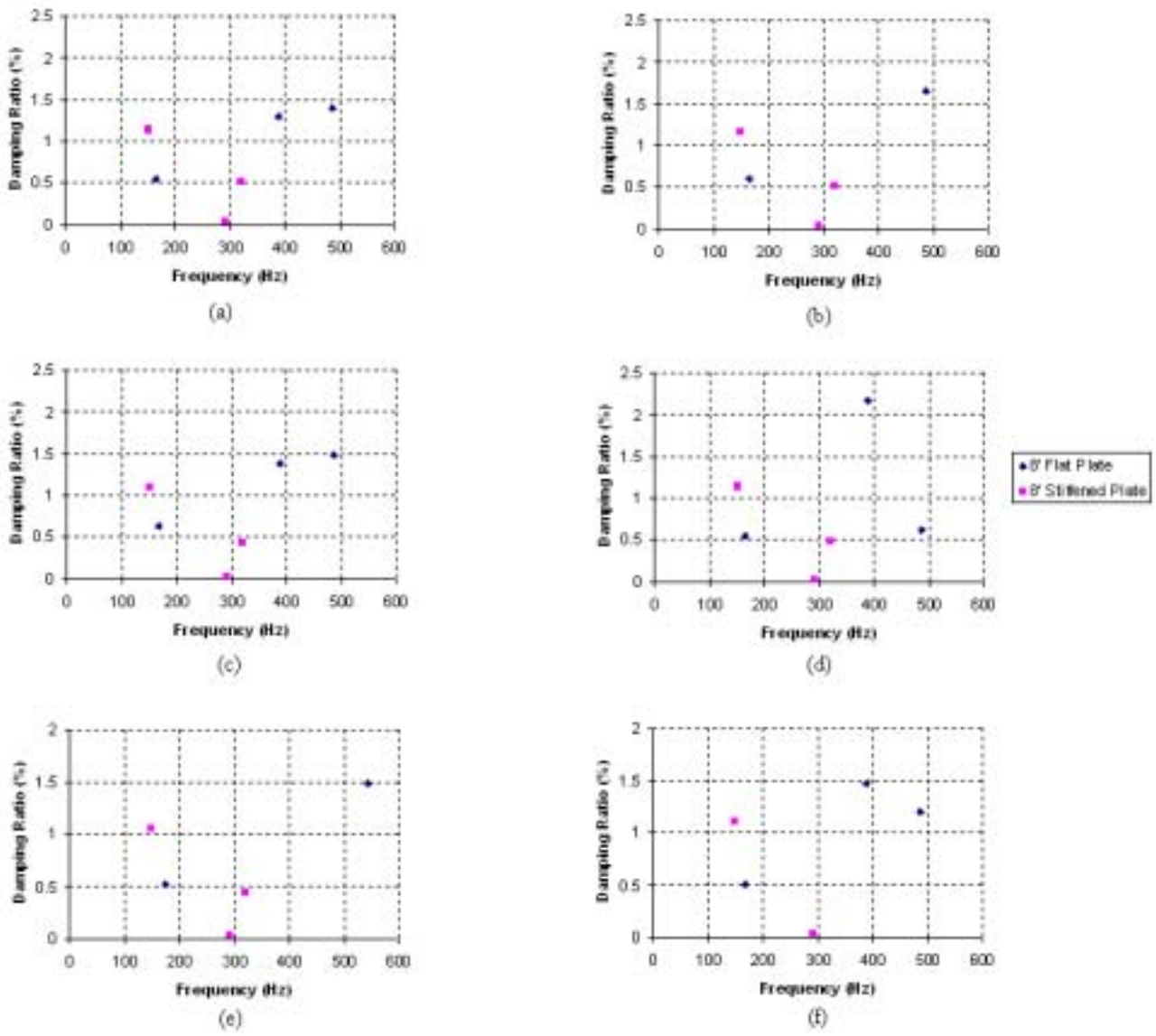

Figure 36. Damping Ratio vs. Frequency response for 8.5-foot plates with one end inserted in sand using the force sensor as the input and accelerometer as the output. (a) measured at location A (b) measured at location B (c) measured at location C (d) measured at location D (e) measured at location D (f) measured at location F.

IV. CONCLUSIONS AND RECOMMENDATIONS

Damping in structures has historically been of great importance in nearly all branches of engineering endeavors, it also happens to be one of the most difficult parameters to predict. Since all modern day combatants are structurally welded together, an understanding of the welding effects is imperative to predicting structural damping. This work examined the welding effects on damping in several beam-stiffened plates.

Unfortunately, with the test structures used this work was unable to present a clear picture of the welding effects on damping for a wide frequency range. At frequencies below 500 Hz the trend observed was that welding caused damping to increase. As the results showed, at some points, the flat plates experienced higher damping ratios than the stiffened plates, which is contradictory to what was expected. In a damping study done by Steven Rutgerson, he found that the damping ratio of bulkheads varied from approximately 2.1% to 8.5% with an average of 4.65% [12]. Of course, a ship structure is much different than the test structures used, but the wide scatter observed on DDG 81 can also be observed in the test structure to a lesser degree.

Recommendations for future work will be to test a more complicated structure that contains a larger amount of welding and that better represents a shipboard structure. The effects of painting and lagging material placed on the bulkhead should also be investigated. Attempts to better simulate the welded region in numerical simulations will enhance the results of the finite element model.

THIS PAGE INTENTIONALLY LEFT BLANK

LIST OF REFERENCES

1. R.M. Grice and R.J. Pinnington, 2000 *Journal of Sound and Vibration*, 825-849. "A Method for the Vibration Analysis of Built-up Structures, Part I: Introduction and Analytical Analysis of the Plate-stiffened Beam."

2. R.M. Grice 1993 *M.SC. Thesis, University of Southampton*. "Vibrational Power Transmission Through Ship Hull and Double Bottom Structures."

3. R.M. Grice and R.J. Pinnington, 2000 *Journal of Sound and Vibration*, 851-875. "A Method for the Vibration Analysis of Built-up Structures, Part II: Analysis of the Plate-stiffened Beam Using a Combination of Finite Element Analysis and Analytical Impedances."

4. R.M. Lin, M.K. Kim and H. Du, 1994 *Computers and Structures* Vol. 52 No. 5 905-915. "A New Complex Inverse Eigensensitivity Method for Structural Damping Model Identification."

5. Y.S. Shin, J.C. Iverson and K.S. Kim, *Journal of Pressure Vessel Technology 1991 Trans. ASME* Vol. 113. "Experimental Studies of Damping Characteristics of Bolted Joints for Plates and Shells."

6. K.K. Padmanabham, 1992 *Journal of Mechanical Tools Manufacuring*. Vol 32 No. 3, 305-314. "Prediction of Damping In Machined Joints."

7. C.V. Betts, R.E.D. Bishop and W. G. Price, 1976 *The Royal Institution of Naval rchitects*. "A Survey of Internal Hull Damping."

8. C.M. Harris, "Shock and Vibration Handbook", 4th Ed., McGraw-Hill 1995.

9. Thomson W.T. and M.D. Dahleh, "Theory of Vibration With Applications", 5th Ed., Prentice-Hall Inc, 1998.

10. Hewlett-Packard Co., *3562A Dynamic Signal Analyzer Operating Manual*, Hewlett-Packard Co., 1985.

11. Wilcoxon Research, 1985, "Wilcoxon Research, Instruction Manual, Model F7/F4 Piezoelectric /Electromagnetic Vibration Generator System."

12. S. Rutgerson, "DDG Damping Study Summary", NSWCCD/UERD Code 661, July 2002.

THIS PAGE INTENTIONALLY LEFT BLANK

INITIAL DISTRIBUTION LIST

1. Defense Technical Information Center
   Ft. Belvoir, Virginia

2. Dudley Knox Library
   Naval Postgraduate School
   Monterey, California

3. Young W. Kwon
   Naval Postgraduate School
   Monterey, California

4. Young S. Shin
   Naval Postgraduate School
   Monterey, California

5. Fred Costanzo
   NSWC Carderock Divison
   Washington, DC

6. Mike Campbell
   NSWC Carderock Divison
   Washington, DC

7. Steve Rutgerson
   NSWC Carderock Divison
   Washington, DC

8. Agustin Carey
   Naval Postgraduate School
   Monterey, California